TABLE OF CONTENTS, Vol. 38, No. 1

SYMPOSIUM ON IRON-BASED CATALYSTS FOR COAL LIQUEFACTION

Small Particle Catalysts

(I. Wender, M. Farcasiu and G. P. Huffman, Organizers,
G. P. Huffman, Presiding; Monday Morning)

Mechanisms

(Continued, I. Wender, Presiding; Monday Afternoon)

TABLE OF CONTENTS, Vol. 38, No. 1

THE DEVELOPMENT OF A NEW IRON CATALYST FOR THE DIRECT LIQUEFACTION OF COAL

Robert BACAUD*, Michelle BESSON* and Gérald DJEGA-MARIADASSOU+

* C.N.R.S., Institut de Recherches sur la Catalyse
2, Av. Albert Einstein, 69626 Villeurbanne cedex, France
+ Laboratoire de Réactivité de Surface et Structure
Université P & M Curie, 75232 Paris cedex 05, France

Keywords: ultra-fine iron catalysts, iron oxide sulfidation, coal liquefaction.

INTRODUCTION

The present paper is a synthesis of the research conducted in a program for the development of iron based catalysts, as a part of a project supported by French government and E. C. between 1980 and 1990. The objective was to provide an evaluation of the feasibility of producing substitute natural gas and liquid transportation fuels, through liquefaction of coal. The development of liquefaction catalysts was performed at laboratory scale in our Institute and the testing of dispersed iron based catalysts was conducted in a 50 kg/d facility at CERCHAR (Charbonnages de France).

The eventual influence of a catalyst upon coal dissolution is a-priori questionable. However, considerable experimental evidence has been accumulated that demonstrates the ability of hydrogenation catalysts to increase the production of soluble compounds from coal at relatively low temperature. This conversion coincides with some hydrogenation which is also enhanced by catalysts. Although low temperature liquefaction cannot generate radical species through homolytic bond cleavage, some coal macerals - especially inertinite - contain significant concentration of free fossil radicals. The initial dissolution process makes these species accessible for further reaction and condensation. The role of catalysts in these conditions is to provide a source of active hydrogen in order to cap these radical species and to avoid retrogressive reactions.

At higher temperature, the rate of radical production increases, as well as the rate of the concomitant reactions of homolytic rupture and condensation, respectively responsible for the formation of gases and insoluble products. A fast stabilization of radical species through hydrogenation contributes to an improvement of selectivity for the production of distillate by reducing the formation of gases and solid residues. A hydrogenation catalyst will prove useful for process control at increased severity but it must demonstrate its usefulness, since it operates in a highly competitive medium where several species can assume some role in hydrogen transfer mechanisms; the more serious competitor for any additional catalyst is the pyrite contained in coals, activity of which is undeniable.

The choice of a catalyst destined to be used in the form of a flowing disposable solid is dictated by the difficulty, even the impossibility, to recover a catalytic substance mixed with unconverted coal and mineral matter. This choice implies a set of requirements must be fulfilled by the catalytic material:

- As an unrecovered reactant, its cost must be low. This primary consideration has considerably limited the range of investigated candidates.
- The solid catalyst is flowing along with the reactants. It is therefore necessary to reduce the amount of displaced substance, both for avoiding the

transport of useless material and for limiting the problems associated with sedimentation and abrasion of reactor and equipments.

- A low catalyst-to-coal ratio imposed by process optimization means the active phase must exhibit a high intrinsic activity.

We decided to develop a synthetic method for the production of a catalyst, considered as the only way of ensuring a proper control of the properties, choosing iron as the cheapest raw material. Among transition metals sulfides, iron is not extremely active (1); its low intrinsic activity must be compensated by a high dispersion. The next step of our program consisted in an investigation of the methods of preparation of highly dispersed iron oxides, considered as precursors for the in-situ generation of iron sulfide during coal liquefaction.

PRODUCING THE CATALYST PRECURSOR

The methods of preparation of heterogeneous catalysts attempt to increase the surface area of the solids. The easiest way consists in producing a porous substance or in supporting the active phase on a porous support. Our first approach consisted in comparing the properties of catalysts obtained by means of deposition of iron compounds on various high surface area supports.

Table I. Characteristics and liquefaction behavior of supported iron oxides

Support	BET $S.m^2.g^{-1}$	Pore radius nm	H increment $\chi^{(a)}$
Carbon black	115	Non porous	0
SiO_2	100	15	0
Al_2O_3	100	20	0
SiO_2-Al_2O_3	600	3	8

(a): relative increment of hydrogen incorporation in coal products as compared to a non catalytic experiment.

Table I clearly illustrates the fact that an active phase, well dispersed on the porous structure of a high surface support, is completely inactive for hydrogen transfer reactions. From these results, it was evident that our attempts should be oriented towards the preparation of high *external* surface area iron solids. We prepared pure iron oxides by precipitation from a nitrate solution with ammonia and we tried to increase the surface by introducing small amounts of various textural promoters, coprecipitated along with iron hydroxide. Only alumina provided some positive effect upon the surface area and liquefaction activity of these solids. A change in the drying process produced a major impact than the introduction of textural promoter as illustrated by table II.

It appeared that hydrogen transfer activity in coal liquefaction is not directly correlated with surface area of the active phase but with the changes in morphology of the particles induced by spray drying.

Ours investigations turned towards the methods of preparation of highly dispersed, non porous solids. A rather simple method consisting in the hydrolysis of volatile compounds in a hydrogen-oxygen flame, currently used for commercial scale production of aerosol oxides of aluminium, silicium and titanium, had been recently adapted to the elaboration of iron oxide (2). Spherical particles are obtained with narrow particle size distribution. The mean particle size can be as small as 10 nm and can be varied through control

of the respective flows of metallic compound vapors and of the gases in the torch. The properties and liquefaction behavior of these catalysts are presented in table II.

Table II. *Characteristics and liquefaction behavior.* Unsupported iron oxides

Catalysts	Drying	BET $S.m^2.g^{-1}$	H increment %(a)
Precipitated oxides			
Fe_2O_3	Oven	150	10
Fe_2O_3	Spray	160	15
Fe_2O_3-$Al_2O_3$10%	Oven	270	4
Fe_2O_3-$Al_2O_3$10%	Spray	200	18
Aerosol iron oxides			
Lab. scale 1		40	18
Lab. scale 2		32	18
Pilot		24	12

(a): Relative increment of hydrogen incorporation in coal products as compared to a non catalytic experiment.

SULFIDATION OF IRON OXIDE

The oxides obtained in a convenient divided state are the precursors of the actual catalytic phase, which results from the interaction of iron oxide with the reacting medium during liquefaction. Owing to the sulfur content of the majority of coals, the partial pressure of hydrogen sulfide can be expected to range around 0.5-2 % in the gas phase during liquefaction. During the early stage of liquefaction, before hydrodesulfurization of coal takes place, the catalyst precursor will be in contact with a highly reducing medium with low initial concentration of hydrogen sulfide; the release of sulfur from coal progressively modifies the composition of the gas phase.

Preliminary experiments revealed that iron oxide is easily transformed into a pyrrhotite $Fe_{0.91}S$ at moderate temperature under hydrogen sulfide partial pressure ranging from 0.2 to 1% in hydrogen (3). Although sulfidation produces a severe decrease of surface area, the resulting phase is active in the reaction of tetralin dehydrogenation in the presence of hydrogen sulfide (Table III).

Table III. Characterization and catalytic activity of iron sulfides generated by gas phase sulfidation of an unsupported iron oxide (BET S.= $24m^2.g^{-1}$)

Treatment	Phases	BET S. $m^2.g^{-1}$	Activity $mol.g^{-1}.s^{-1}$(a)
1 - H_2S	$Fe_{0.91}S$	3	4.10^{-8}
2 - H_2	$Fe_{0.995}S$	3	$0.3.10^{-8}$
1 - H_2	Fe	2	10.10^{-8}
2 - H_2S	$Fe_{0.995}S$	0.1	$0.1.10^{-8}$

(a) Catalytic activity in dehydrogenation of tetralin at 600 K, 0.1 MPa H_2

A reduction of this sulfide under hydrogen generates a considerably less active phase, identified as $Fe_{0.995}S$. A preliminary reduction of iron oxide under hydrogen produces a very active metallic phase. Partial sulfidation of metallic iron completely inhibits its activity. The production of $Fe_{0.995}S$ by

sulfidation of metallic iron by hydrogen sulfide is very progressive and gives rise to a drastic sintering (4).

This study was completed by an examination of the influence of the protocol of sulfidation and introduction of the catalyst in the reacting medium during coal liquefaction, in the presence of a hydrogen-donor solvent (tetralin). We compared the ability of catalysts to rehydrogenate the solvent, after different sulfidation protocols described below.

- In-situ sulfidation: the catalyst precursor is introduced into the reactor along with the reactants and sulfur, then heated up to the reaction temperature.
- Pre-sulfidation: either in the gas phase, by a mixture containing 1 % hydrogen sulfide in hydrogen, or in suspension in tetralin under 1 % H_2S in H_2 at 15 MPa total pressure.
- Flash-sulfidation: the precursor is introduced under pressure (15 MPa) in the autoclave containing the reacting medium (coal, solvent, H_2S and H_2) at reaction temperature.

As evidenced in table IV, only catalysts pre-sulfided in gaseous H_2S or in-situ sulfided are active for solvent hydrogenation. The drastic reduction of activity caused by a pre-sulfidation in tetralin suggests that coal itself must interfere with the process of generation of the active phase from iron oxide.

Table IV. Influence of sulfidation protocol upon solvent hydrogenation during coal liquefaction (tetralin 673 K, 1%H_2S)

Protocol	% Solvent dehydrogenated
In-situ	2
Gas phase pre-sulfidation	3
Liquid phase pre-sulfidation	13
Flash sulfidation	13
No catalyst	13

A systematic electron microscope examination, associated with X-ray emission micro-analysis, revealed an agglomeration of sulfide particles when the precursor was sulfided in the absence of coal; the surface of the grains was covered with an opaque, thick layer of coke probably resulting from cracking of tetraline (5). On the contrary, samples originating from in-situ sulfidation, in the presence of coal, showed that the sulfided particles preserved the particle shape of the precursor. A smooth carbonaceous deposit was evidenced at the surface of the particles. This layer, as opposed to the dense coke formed in tetralin, preserved the hydrogenation activity (6). It may results from adsorption of dissolved coal products which prevent particles agglomeration.

EVALUATION OF CATALYSTS IN COAL LIQUEFACTION

Using a disposable catalyst prescribes low catalyst-to-coal ratio. An evaluation of catalysts for coal liquefaction must include determining the minimum loading required for a given level of conversion. In this part of our project, we chose conditions of high severity liquefaction, i.e. high temperature and a non-donor solvent. Coke buildup occurs in these conditions for non catalytic experiments. As a tool for catalysts evaluation, we determined the minimum amount of catalyst required for unperturbed reactor operation during 1 hour runs. This arbitrary criterion, designed as "critical catalyst loading", does not attempt to define an absolute value but is

indicative of the relative performances of distinct catalysts. Some of the catalysts included in table V are representative of the improvements we obtained in the synthesis of iron oxide. The effect of increasing external surface area is evidenced, as well as the doping effect produced by incorporation of minor amount of molybdenum.

Table V. Critical catalyst loading

Catalyst	Weight % vs coal
Red mud	2.2
Fe_2O_3, 18 $m^2.g^{-1}$	0.7
Fe_2O_3, 71 $m^2.g^{-1}$	0.4
Fe_2O_3, 2.8 % MoO_3	0.2
Fe_2O_3, 18 % MoO_3	0.2

The influence of catalyst loading on oil yield is presented in Fig. 1 for some representative catalysts. The change in oil production is not proportional to the catalyst content and a twofold increase of catalyst percentage only causes oil yield to vary from about 40% to 50%.

The relation between the amount of hydrogen incorporated into the final liquid coal products and the percentage of catalyst is described in Fig. 2. It must be specified that the values correspond to a net H_2 incorporation and that the contribution of hydrogen to the formation of light gases from the organic matter of coal has been subtracted; increasing the amount of red mud for example, enhances hydrogen consumption, but this additional H_2 is mainly utilized for the production of gases. On the contrary, the net hydrogen incorporation augments with increasing the amount of iron oxide based catalysts, and it reaches higher levels than with Ni-Mo. As indicated above, oil production varies little with the nature and with the percentage of catalyst. Consequently, the hydrogen content of the oils produced in distinct catalytic conditions - and therefore oil quality - must vary accordingly. This is reflected by the percentage of H_2 incorporated into oils or into (oils + asphaltenes) reported in table VI.

Table VI. Weight % H_2 incorporated into oils or asphaltenes

Catalyst (1.5% vs. coal)	H_{oil}	$H_{oil+asphalt}$
Fe_2O_3, 71 $m^2.g^{-1}$	4.44	3.49
Fe_2O_3, 2.8%MoO_3	4.38	4.05
Ni-Mo/Al_2O_3	3.48	2.60
Red mud	3.0	2.15

From a linear regression of the rate of hydrogen consumption versus the pressure decrease, an initial rate of H_2 incorporation could be deduced. The results are presented in Fig. 3. This apparent initial rate reflects the activity of the fresh catalyst. Initial activity for Ni-Mo is superior to that of pure iron oxide, although the products obtained with the former are less hydrogenated; the same is observed concerning the hydrogenation of the solvent (Fig. 4): iron based catalysts exhibit a higher activity than Ni-Mo. Although supported Ni-Mo is intrinsically a better catalyst than iron sulfide (as evidenced by its higher initial activity), its exposed active surface declines rapidly, due to the plugging of the porous structure by carbonaceous deposits. On the contrary, the surface of unsupported iron sulfides is

affected to a less extent by this phenomena, and consequently their activity can maintain at a convenient level.

CONCLUSION

As part of a program for the production of fluid fuels through coal liquefaction, we investigated the pertinent basis for the elaboration of catalytic materials. Considering the requirements imposed by the specific conditions of use of disposable catalysts in coal liquefaction, we decided to prepare synthetic iron based solids. The prominent results of this program are summarized below:

- Catalytic activity relies upon the external surface area. Porous solids that exhibit a high surface are inactive, as compared to non porous ones.
- Nanometer-sized iron oxides (aerosol) can be produced through vapor phase hydrolysis of volatile compounds in a hydrogen-oxygen flame. They exhibit uniform spherical shape particles whose diameter can be as low as 10 nm.
- Sulfidation of these precursors generates a pyrrhotite at moderate temperature. A previous reduction of iron oxide to the metallic state must be avoided, since further sulfidation is considerably more difficult.
- Coal provides a support effect during sulfidation and prevents, up to some extent, the agglomeration of catalyst particles.
- The performances of aerosol iron oxides in coal liquefaction largely exceed those of red mud and compare favourably with commercial supported Ni-Mo catalysts. They can be improved by incorporation of minor amounts of molybdenum.
- Critical catalyst loading, indicative of the minimum catalyst-to-coal ratio compatible with reactor operability, suggests that the proposed catalysts can be used at concentration levels as low as 0.2% vs coal.

ACKNOWLEDGMENTS

H. Charcosset, presently retired, initiated and gave the impulse to this program. His role, as a group leader of the French laboratories included in this project, has been decisive. We wish, by means of this paper, to express our gratitude for his essential contribution.

REFERENCES

(1) Lacroix, M.; Boutarfa, N.; Guillard, C.; Vrinat, M.; Breysse, M., J. Catal. 1989, 120, 473-477.
(2) Vergnon, P.; Batis Landousli, H., Ind. Eng. Chem.- Prod. Res. Dev. 1980, 19, 147-151.
(3) Andrès, M.; Charcosset, H.; Davignon, L.; Djega-Mariadassou, G.; Joly, J.P., Bull. Soc. Chim. France 1982, 11, 427-432.
(4) Zimmer, H.; Andrès, M.; Charcosset, H.; Djega-Mariadassou, G. Applied Catal. 1983, 7, 295-306.
(5) Djega-Mariadassou, G.; Besson, M.; Brodzki, D.; Charcosset, H.; Tran Huu Vinh, Fuel Process. Technol. 1986, 12, 143-153.
(6) Bacaud, R.; Besson, M.; Brodzki, D.; Bussière, P.; Charcosset, H.; Djega-Mariadassou G.; Oberson, M. in: B. Delmon and G.F. Froment (Editors) "Catalysts Deactivation", Elsevier, Amsterdam, 1989, p.289.

Fig. 1: Oil yield
as a function of catalyst loading

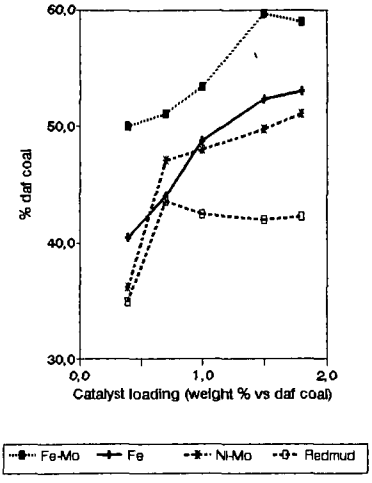

Fig. 2: hydrogen incorporation
in coal liquids

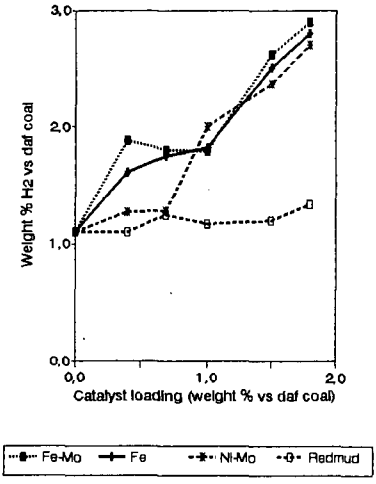

Fig. 3: Initial rate of H2 uptake
Liquefaction 723K, non donor solvent

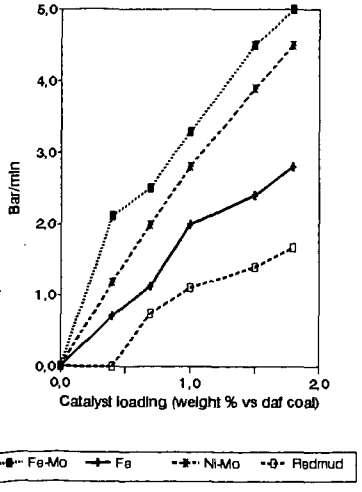

Fig. 4: Solvent hydrogenation
Liquefaction 723K, 1 hr residence time

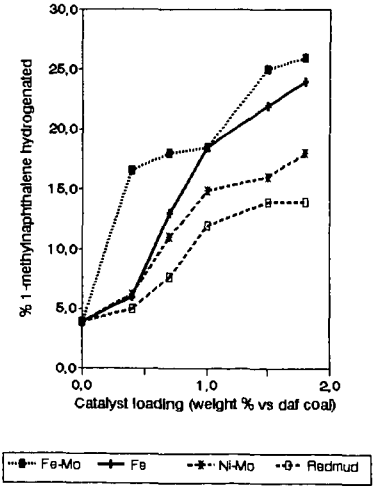

SULFATED AND MOLYBDATED IRON (III) OXIDE CATALYSTS IN COAL LIQUEFACTION

V.R. Pradhan, J. Hu, J.W. Tierney and I. Wender

Chemical and Petroleum Engineering Department
University of Pittsburgh, Pittsburgh PA 15261

Keywords: Sulfated Iron Oxides, Low-Pyrite Coals, Pyrrhotites

INTRODUCTION

Iron, because of its low cost, activity, and environmental acceptability, has been perceived as a potential catalyst for the first stage of coal liquefaction, namely coal dissolution. A chief objective of various methods of adding iron catalysts is to provide high catalytic surface area and fine particulate size. The initial dispersion of the precursor has a strong influence on the activity of the sulfided phases formed under liquefaction conditions. Means must also be sought to prevent agglomeration of catalyst particles so as to maintain their state of high dispersion. In the presence of enough sulfur, iron catalysts form pyrrhotites ($Fe_{1-x}S$) which, along with hydrogen sulfide, function as catalysts for the hydrogenation and hydrogenolysis reactions which occur during the hydroliquefaction of coal[1,2,3]. Application of finely divided and chemically modified powdered solid iron oxide based catalysts used in this work shows considerable promise[4]. These catalysts have initial sizes in the nanophase region (1-100 nm); their ultrasmall size allows them to have dramatically different properties.

The objective of this research has been to use low-sulfur, low-pyrite coals to verify the catalytic effects of small amounts of iron added to the liquefaction reactor as sulfate and molybdate anion-promoted oxides or oxyhydroxides. We have reported on the use of sulfate-promoted iron and tin oxides for the direct liquefaction and coprocessing of Argonne Illinois No. 6 coal with tetralin and with Maya ATB heavy oil, respectively[4].

The following topics will be discussed: (i) activity of small amounts of iron and molybdenum added as sulfated oxides for direct liquefaction of low pyrite coals (hvbC Blind Canyon, 0.01 wt% pyrite, and subbituminous Wyodak with 0.17 wt% pyrite), (ii) synthesis and physicochemical properties of sulfated and other anion-modifed iron oxide/oxyhydroxide catalysts before use in coal liquefaction reactions, (iii) quantification of dispersion and composition of iron phases after coal liquefaction and (iv) transformation and sintering behavior of these catalysts under coal liquefaction conditions.

EXPERIMENTAL

Starting Materials. The hvbC Blind Canyon DECS-17 coal was obtained from the Penn State Coal Sample Bank and the Wyodak subbituminous coal from the Argonne Coal Sample Bank. Elemental analyses are given in Table 1. Starting materials for catalyst preparation were iron alum [$Fe_2(SO_4)_3(NH_4)_2SO_4 \cdot 24H_2O$], ferric nitrate, urea, and 28% ammonia water. Ammonium heptamolybdate and ammonium metatungstate were purchased from the Sigma Chemical Co. and from Strem Chemicals, Inc. respectively.

Catalyst Preparation and Characterization. The sulfated oxides and oxyhydroxides of iron were prepared from either the sulfate or

nitrate salts using urea or NH_4OH as the precipitating agents, added dropwise so that the pH of the solutions changed with time. The result of the hydrolysis reaction is formation of iron oxyhydroxide (FeOOH) with small residual amounts of sulfate anion adsorbed on the surface. The presence of sulfate anions during precipitation has been reported to bring about surface charge modifications of the precipitated particles; this affects the chemistry and kinetics of the precipitation/crystallization. The catalysts used in this study were Fe_2O_3 (I), Fe_2O_3/SO_4 (II), $Mo/Fe_2O_3/SO_4$ (III), $FeOOH/SO_4$ (IV), Fe_2O_3/MoO_4 (V), Fe_2O_3/WO_4 (VI) and $Mo/FeOOH/SO_4$ (VII). These catalysts were prepared by modification of the procedure used for the preparation of Fe_2O_3/SO_4 (II)[4].

The following measurements were made to characterize the size and structure related properties of these catalysts: BET surface area, sulfur content, thermogravimetry (TGA), acidity measurements, thermal stability measurements, X-ray diffraction and electron microscopy. Residues of coal liquefaction experiments were also analyzed using a Phillips X-ray diffractometer and a JEOL 2000 FX STEM (100 kV beam) with an energy dispersive X-ray spectrometer (EDX) to determine composition and dispersion of catalytic phases formed under liquefaction conditions.

Reaction Studies. Tetralin was the reaction solvent (3:1 by weight to coal) and elemental sulfur (2:1 by weight to catalyst) was used for *in situ* catalyst sulfidation. Although a donor solvent such as tetralin tends to mask catalytic effects in coal conversion, its presence during coal liquefaction ensures complete conversion of the iron catalyst precursor to its sulfide via H_2S formation in 5-6 minutes at 400°C at 1000 psig cold H_2. Coal liquefaction reactions were carried out in in both a 300 cc stainless steel autoclave and a 27 cc tubing bomb microreactor at 400°C and 1000 psig ambient H_2 (1800 psig at reaction temsperature). Coal conversions were determined using Soxhlet extraction with methylene chloride; soluble products were recovered by evaporation at 45°C under vacuum. Pentane solubles (oils) were determined by Soxhlet extraction of the methylene chloride solubles with n-pentane. Asphaltenes are the pentane-insoluble but methylene chloride soluble material.

RESULTS AND DISCUSSION

Catalyst Synthesis and Characterization. The catalysts used are listed in Table 2 with relevant physicochemical properties. The presence of sulfate anions during precipitation was necessary to form nano-sized oxide particles which were resistant to agglomeration at high temperature.

The measure of initial dispersion of the catalysts was obtained using XRD line broadening measurements and transmission electron microscopy (TEM). The crystallite sizes of sulfated iron oxyhydroxides could not be determined by X-ray diffraction due to their low bulk crystallinity. These oxyhydroxides, after calcination, gave rise to catalyst II (high bulk crystallinity). Use of TEM revealed that catalyst IV contained very small needle-shaped, elongated, thin crystallites with average dimensions of 30 x 3 nm. Nitrogen porosimetry measurements were carried out on all catalysts. A macroporous distribution of pores was obtained for catalyst IV, indicating that individual fine particles come together to form very thin channels with average dimensions of 20-30 nm. All calcined iron oxides, completely crystalline after calcination, were 10-15 nm and

were elongated in shape as determined by electron microscopy.

The uncalcined sulfated oxyhydroxides such as IV had BET specific surface areas (120-130 m^2/g) higher than the calcined oxides (80-90 m^2/g). Evidence that all of the sulfated iron oxides had low porosities with pore volumes smaller than 0.2 cc/g was obtained by calculating equivalent spherical diameters from their surface area values and comparing them with diameters obtained by TEM. The values agreed within 10%.

The iron oxide surfaces were studied by FTIR and XPS. The FTIR spectrum of catalyst IV, obtained at 450°C under vacuum, showed an S=O band at 1440 cm^{-1} similar to the S=O bonds formed in the bidentate chelating complex of sulfate anion with an oxide surface proposed by Tanabe et al.[5] Upon adsorption of pyridine, this band shifted to about 1500 cm^{-1} and new bands, corresponding to coordinatively bonded pyridine (Lewis acid sites) and to pyridinium ions (Bronsted acid sites) appeared in the spectrum. XPS of the sulfated and molybdated iron oxides indicated that almost 95% of the S and Mo , both in 6+ oxidation states, were on the catalyst surface.

Reaction Studies. Coal liquefaction reactions were carried out both in a horizontally shaken tubing microreactor and a well-stirred 300 cc batch autoclave. Blank (thermal) runs were made with a previously unused microreactor to determine the catalytic activity of inherent mineral matter in the coals. Runs were also made with only elemental sulfur added to the reactor without added catalyst. Catalysts were mixed with the coal-tetralin slurry by manual stirring after being preheated in an oven at 450°C for one hour. Liquefaction experiments with sulfated iron oxides, presonicated in the reaction solvent for one hour, were also carried out; this treatment ruptured the catalyst agglomerates (about 1 nm as determined by light scattering) into smaller particles which formed a stable colloidal suspension in tetralin, thereby increasing the extent of initial catalyst dispersion.

Comparison of Catalytic Activities of Sulfated Iron Oxides and Oxyhydroxides with other Finely Divided Catalyst Precursors. Use of catalysts IV and VII (both uncalcined) resulted in total coal conversion levels similar to those obtained with their calcined forms (II and III), although higher oil yields were obtained with the calcined forms. The higher activity of calcined iron oxides for oil production is probably related to their calcination treatment at 500°C for three hours. The higher water content of the oxyhydroxides may make them more susceptible to sintering during transformation to pyrrhotites.

Activities of sulfated iron oxides were compared with those of organometallic precursor complexes such as $Fe(CO)_5$ and $Mo(CO)_6$ as well as with a fine divided (30 Å) iron oxide catalyst. Catalyst II was more active than $Fe(CO)_5$ at the same iron loading. Interestingly, 500 ppm of Mo (added as either $Mo(CO)_6$ or molybdenum naphthenate) relative to coal resulted in about the same conversion levels as 3500 ppm of Fe added as catalyst II.

Coal Conversion and Oil Yields as a Function of Catalyst Concentration. Coal conversions were carried out using the smallest catalyst loadings that gave meaningful results. Since most coals contain considerable amounts of iron as FeS_2, it is difficult to obtain reliable data on the effect of small catalyst loadings on coal conversion levels. Two coals with low levels of iron, a Blind Canyon

coal with 0.02 wt% of pyrite and a Wyodak coal with 0.17 wt% of pyrite were selected to minimize the effect of inherent mineral matter. Uncalcined catalyst IV, which was as active as the calcined catalyst II, was employed for runs carried out to determine the effect of small loadings of iron (1000-5000 ppm with respect to coal) on coal conversion and on oil yields. With the Blind Canyon coal, a thermal blank conversion of 60% (maf) and oil yield of 22% were obtained. With 3500 ppm of Fe as catalyst II, conversion increased to 77% and oils to 35%. The highest conversion (87% with 48% oils) was achieved with 1% of $FeOOH/SO_4$ (IV).

The effect of Mo loadings (20-200 ppm with respect to coal) used with 2500 ppm of iron as III was investigated. Very small amounts of Mo added to II enhanced coal conversion from 72% to 80%; the yield of oils, however, rose from 32% without Mo to 46% with 100 ppm of Mo. On increasing Mo loading to 200 ppm, total conversion was 87% and yield of oils 52%. The molybdenum in catalyst III probably forms MoS_2, which has a strong hydrogenation function so that more oil is produced at the expense of asphaltenes.

Effect of Different Anionic Modifications of Iron (III) Oxides on Coal Liquefaction Activity. Iron oxides modified with 5 wt% of molybdate (MoO_4) or tungstate (WO_4) anions were as active as sulfated iron oxide catalysts in terms of overall coal conversion.

All runs with the Blind Canyon coal were made with addition of elemental sulfur to the reactor. Use of S alone in a blank run (no catalyst added) resulted in 66% coal conversion with 27% oils. Iron oxides modified with either tungstate or molybdate anions resulted in slightly higher oil yields than the sulfated iron oxide. The higher activity is due to formation of highly active and well dispersed MoS_2 or WS_2. These new types of anionic modifications of iron oxides bring about significant enhancement in coal liquefaction activity.

Catalyst Presulfidation and Re-use. To establish the activity of highly dispersed pyrrhotites formed from the sulfated iron oxides, we carried out presulfidation instead of *in situ* sulfidation of the catalysts by reacting them with 2:1 (by weight) of S in the presence of tetralin at 400°C and 1000 psig H_2 cold for 30 minutes in the 300 cc autoclave. X-ray and electron diffraction indicated that all sulfated iron oxides were converted to Fe_7S_8 with traces of $Fe_{11}S_{12}$. X-ray line broadening measurements and transmission electron microscopy indicated a crystal size of 20 nm for these preformed pyrrhotites, which, interestingly, contained 3 to 5 wt% of carbon derived from the solvent tetralin. The tetralin was found to have been hydrocracked, hydrogenated, and dehydrogenated during presulfidation of the sulfated catalysts.

The preformed pyrrhotites were then employed as catalysts for direct liquefaction of Blind Canyon coal at 400°C at 0.25 to 0.35 wt% iron loading relative to coal both with and without added S. The preformed Fe_7S_8 was almost as active as catalyst IV at 0.35 wt% iron. Further addition of S to Fe_7S_8 improved its activity, yielding 42% oils compared to 30% with larger amounts of Fe_7S_8 in the absence of added S with 2500 ppm of iron. Increase in oil yields upon addition of S to Fe_7S_8 indicates possible interactions between pyrrhotites and H_2S for catalyzing hydrogenolysis/hydrogenation reactions during coal liquefaction. The presence of H_2S also ensures that the iron-deficient and sulfur-rich stoichiometry of pyrrhotites is maintained.

Effect of Reaction Temperature. Catalysts I, II and III were used for liquefaction of Wyodak coal at 375, 400, and 425°C. The activities of these catalysts for production of oils from coal increased on going from 375 to 425°C except for the Fe_2O_3 (I) catalyst, for which oils decreased somewhat. Sulfated catalysts resulted in higher yields of oils than the unsulfated ones at all temperatures.

Dispersion and Composition of Catalysts after Coal Liquefaction. To study what happened to initially added iron catalyst precursors after coal liquefaction, we carried out reactions of Blind Canyon coal with II and with $Fe(CO)_5$. The insoluble residues containing transformed iron catalysts were characterized by X-ray diffraction and STEM coupled with an Energy Dispersive X-ray Detector. The added iron for both precursors was completely converted to pyrrhotities, highly dispersed in the insoluble organic matter in the liquefaction residue. Pyrrhotites formed from $Fe(CO)_5$ were larger (30-50 nm) than those from II (15-20 nm).

CONCLUSIONS

1. Sulfated iron oxides and oxyhydroxides and molybdenum promoted sulfated iron oxide were active for converting low pyrite coals to liquids at 400°C; coal conversion levels greater than 75%, compared to 66% without catalyst, were obtained with iron loadings between 2500-5000 ppm relative to coal.
2. The sulfate, molybdate and tungstate anions modified the physicochemical properties of iron(III) oxides in a similar way and were about equally effective for direct liquefaction of low-pyrite Blind Canyon coal, but slightly higher yields of oils were obtained with iron oxides promoted by molybdate or tungstate.
3. Uncalcined sulfated iron oxyhydroxides were almost as active as the calcined sulfated iron oxides, but somewhat higher amounts of oils were obtained using calcined oxides. Although initially both oxides and oxyhydroxides are highly dispersed, sulfated oxides resist sintering at high temperatures. Uncalcined sulfated oxyhydroxides have residual moisture which is probably responsible for agglomeration under coal liquefaction conditions.
4. Iron, in the form of sulfated oxides, is completely converted to highly dispersed pyrrhotites within a few minutes at 400°C. These have a composition of Fe_7S_8 and an average particle size of 20 nm. No growth in particle size during reaction was observed. The presulfided Fe_7S_8 is also active for direct liquefaction of coal in the presence of added sulfur.
5. A catalyst system based on anion-modified iron oxides has an initial fine size and a unique ability to resist agglomeration at higher temperatures.

ACKNOWLEDGMENTS

The authors acknowledge financial support from the United States Department of Energy under award DE-FC22-90PC900029 and the Exxon Education Fund. Contributions of coal samples by the Argonne Premium Coal Sample Bank and the Penn State Coal Sample Bank are also acknowledged.

REFERENCES

1. Trewhella, M.J. and A. Grint, *Fuel*, **1987**, **66**, pp, 1315-1219.
2. Baldwin, R.M. and S. Vinciguerra, *Fuel*, **1983**, **62**, pp 498-501.
3. Ogawa, T., V.I. Stenberg and P.A. Montano, *Fuel*, **1984**, **63**, pp. 1660-1663.
4. Pradhan, V.R., J.W. Tierney and I. Wender, *Energy & Fuels*, **1991**, **5**, pp 497-507.
5. Tanabe, K., H. Hattori, T. Yamaguchi, T. Iizuka, H. Matsuhashi, A. Kimura and Y. Nagase, *Fuel Proc. Tech.*, **1986**, **14**, pp 247-260.

Table 1. Ash-free Elemental Analyses of Coals (weight percent)

Coal	Carbon	Hydrogen	Nitrogen	Oxygen	Sulfur	Pyritic Sulfur
Wyodak	75.0	5.4	1.1	18.0	0.5	0.17
Blind Canyon	81.6	6.2	1.4	10.3	0.5	0.002

Table 2. Catalyst Characterization before Reaction

Catalyst[1]	Wt % SO_4	Surface Area, m^2/g	Average Size, nm		
			XRD	TEM	ESD[2]
I	0.0	26.8	46	65	41
II	3.4	81.7	12	20	14
III	3.1	81.5	12	20	14
IV	10.2	127.0	nd	16	11
V	0.0	88.0	9	15	13
VI	0.0	91.5	7	15	12
VII	9.8	120.5	nd	20	11

1. Molybdated and tungstated iron (III) oxides contained 5 wt% molybdate or tungstate.
2. ESD is the equivalent spherical diameter of the catalyst particles, calculated from the BET surface area and assuming zero porosity.

PREPARATION OF ULTRAFINE CATALYST POWDERS USING A FLOW-THROUGH HYDROTHERMAL PROCESS

Dean W. Matson, John C. Linehan, and John G. Darab
Pacific Northwest Laboratory,
P.O. Box 999, Richland, WA 99352.

Keywords: Catalyst synthesis, Iron catalysts, Catalyst characterization

ABSTRACT

The rapid thermal decomposition of solutes (RTDS) process was used to produce ultrafine iron-bearing oxide and hydroxide powders for use as coal liquefaction catalysts. The RTDS process subjects aqueous solutions containing dissolved metal salts to elevated temperatures and pressures in a flow-through apparatus. Particle formation is initiated during brief exposure of the solution to a heated region, then is quenched by abruptly cooling and depressurizing the suspension. Powders having individual crystallites on the nanometer to tens-of-nanometer size scale are readily produced by the RTDS method. Variations in RTDS processing parameters (e.g., solute concentration, flow rate, processing temperature) affect the crystallinity, morphology, and size of particles produced. Powders generated using the RTDS process were characterized using XRD, EXAFS, electron microscopy, Mossbauer spectroscopy, and BET surface area analysis.

INTRODUCTION

The development of inexpensive and environmentally benign materials exhibiting catalytic activity toward coal liquefaction processes will enhance the economic viability of coal liquefaction as a source of liquid transportation fuels. If active materials can be developed which meet these criteria, the application of single-use "throw away" catalysts will eliminate the need for costly catalyst reclamation steps in the liquefaction process. Inexpensive iron-based materials have been shown to be catalytically active in coal liquefaction processes, although their activities are typically low compared to other, much more expensive and/or toxic molybdenum-based materials.[1] One approach which can be taken to counteract the inherently lower catalytic activity of iron-based materials is to increase the surface site availability per unit weight of catalyst. The production of finely divided catalyst precursor powders having particle sizes on the nanometer to tens of nanometer size scale offers specific surface areas of up to several hundred m^2/g. In addition to the increase in availability of active sites, ultrafine particles have a much higher mobility within the reaction medium, increasing the potential for coal/catalyst contact.[2]

We have shown that ultrafine iron-bearing particles can be generated quickly in a flow-through hydrothermal process referred to as the rapid thermal decomposition of solutes (RTDS) process.[3] The RTDS process offers a method of generating both ultrafine iron (hydroxy) oxides and mixed metal (hydroxy) oxides using inexpensive water soluble precursors. The RTDS process is amenable to variations in a number of processing parameters. Among those readily adjusted are the precursor salt and its concentration in solution, the processing temperature and pressure, and the length of exposure to the heated region. In this report we present the results of efforts to characterize iron-bearing powders generated using the RTDS method and to relate the effects of varying processing parameters on the powder characteristics. Results of catalytic activity runs using RTDS products are presented in a companion paper.[4]

EXPERIMENTAL

Details of the RTDS powder formation method have been presented elsewhere[3] but are summarized here for convenience. As it is used for the preparation of iron-bearing powders from aqueous solutions, the RTDS technique involves rapid transport of the precursor solution through a high temperature, high pressure region followed by an abrupt transition to low temperature and

ambient pressure. Solutions were pressurized using a high pressure reciprocating piston pump and subsequently passed through a length of stainless steel tubing which was resistively heated using the temperature regulated output from a DC power supply. Temperatures of the solutions at the downstream end of the heated tube were monitored by a thermocouple mounted in the fluid flow. Typical fluid residence times in the heated region of the apparatus were less than 2 seconds. After passing through the heated tube, the solution was depressurized by passing it through a small orifice. The resulting spray was directed into a flask immersed in an ice bath, where the resulting suspension was collected. For the purposes of investigating the RTDS process as a method of ultrafine powder production, a standard metals concentration of 0.1 M was chosen for the feed solutions.

Iron-bearing RTDS suspensions were separated by allowing the particulate fraction to settle, either gravitationally or by centrifugation. If required, additional salts were added to the suspensions to flocculate the particles and assist the settling process. Liquid above the particulate layer was decanted off, the particles were washed with deionized water, and the process was repeated. The resulting solid product was dried under flowing nitrogen or air.

A variety of techniques were used to characterize the RTDS-generated powder products. Powder X-ray diffraction (XRD) was routinely used to determine crystalline phases present in the RTDS powder product, and XRD line broadening analysis provided crystallite size data. Selected samples were also analyzed using Mossbauer spectroscopy, BET nitrogen adsorption analysis, extended X-ray absorption fine structure (EXAFS) spectroscopy, and electron microscopy.

RESULTS and DISCUSSION

In the absence of other components, ferric nitrate solutions processed using the RTDS method yielded deep red to red-brown suspensions characteristic of polymeric ferric oxides and hydroxides.[5] The 0.1 M $Fe(NO_3)_3$ solutions processed at RTDS temperatures above 250°C formed solids which settled readily, while those produced at lower temperatures (200-250°C) settled much more slowly or remained suspended until salted out.

The pH of the 0.1 M $Fe(NO_3)_3$ solutions was roughly 2.0 as prepared, and dropped approximately 0.3 pH units during the RTDS processing. This decrease in pH resulted from hydrolysis reactions occurring under the hydrothermal conditions present in the RTDS apparatus:

$Fe^{3+} + 2H_2O \longrightarrow FeOOH + 3H^+$ and $2Fe^{3+} + 3H_2O \longrightarrow Fe_2O_3 + 6H^+$. Efforts to modify the pH of RTDS solutions by adding an acetate buffer (0.36 M sodium acetate and 0.04 M acetic acid) raised both the before- and after-processing pH values above 4.0. Processing of the buffered solution at low temperature (225°C) generated a dark reddish brown suspension that did not settle, although a solid product was salted out by addition of sodium sulfate.

The analytical results from iron (hydroxy) oxide powders produced by RTDS processing of aqueous 0.1 M $Fe(NO_3)_3$ solutions at various temperatures are summarized in Table 1. These results suggest that at low processing temperatures (< 250°C), the phase obtained was 2-line ferrihydrite or mixtures of ferrihydrite and hematite (α-Fe_2O_3). Both XRD and transmission electron microscopy (TEM) analyses indicated that these low-temperature RTDS products consisted of powders containing crystallites smaller than 10 nm in diameter. Higher RTDS processing temperatures (300-400°C) yielded the hematite form of iron oxide exclusively, and crystallite sizes were observed to increase as a result of higher processing temperatures (Fig. 1, Table 1). The increase in crystallite size with increasing RTDS processing temperature was also reflected in the room temperature Mossbauer spectra of the powder products as a shift from the 2-line quadrupole doublet spectrum characteristic of particles less than 8.5 nm in diameter to the 6-line hyperfine spectrum which is characteristic of bulk hematite (Fig. 2).[5,6]

Figure 3 shows plots of the iron nearest neighbor shell radii (uncorrected for phase shift) determined from the iron K-edge EXAFS spectra of the powders produced from 0.1 M ferric nitrate solutions as a function of increasing RTDS processing temperature. At the lowest RTDS temperature (200°C), the nearest neighbor shell radii are indicative of low molecular weight oligomers. As the RTDS temperature is increased, the radii approach those which are representative of bulk hematite (2.730 Å for iron and 1.473 Å for oxygen).

The effect of adding urea (1.0 M) to ferric nitrate solutions being processed by the RTDS method was also investigated (Table 1). Decomposition of the urea to carbon dioxide and ammonia at RTDS processing temperatures resulted in a rapid rise in solution pH simultaneously with the development of hydrothermal conditions, producing a competing cation precipitation mechanism. Little effect was noted below 250°C because, at the short residence times of the solutions in the elevated temperature region of the RTDS apparatus, the decomposition of the urea was insufficient to significantly change the solution pH. At 250°C and 300°C RTDS temperatures the pH of the processed solutions was above 8.5, and the product was a reddish brown opaque gel. XRD analysis of the solid product indicated the presence of a poorly crystallized material, consisting primarily of 6-line ferrihydrite.

Catalytic activity and/or selectivity of ultrafine iron oxides may be significantly affected by the doping of other metals into the solid matrix.[1] Consequently, the production of iron oxide powders doped with other cations by co-precipitation during RTDS processing was investigated. Results of representative RTDS runs using additional cationic species as dopants are presented in Table 2. Empirically, the results obtained from the runs containing dopants were consistent with the results of ferric iron-only runs, although some differences were detected in secondary iron oxide phases which were produced. The principle phases identified in the resulting products were those of hematite and 6-line ferrihydrite (a hematite precursor). 2-line ferrihydrite may also have been present in some samples, but was not identified due to the weakness of its XRD pattern relative to that of the other phases. Some additional phases were identified in samples in which urea had been added to the feed solutions.

Efforts at obtaining magnetite (Fe_3O_4) by processing a solution containing both Fe^{3+} and Fe^{2+} salts yielded only hematite and ferrihydrite phases under the conditions investigated, with the relative concentration of those phases dependent on the processing temperature. At 225°C the mixed iron system yielded both hematite and 6-line ferrihydrite, although only 2-line ferrihydrite was observed in the product of ferric nitrate only runs at similar processing conditions. At higher processing temperatures the relative concentration of hematite to 6-line ferrihydrite increased until at 400°C the product obtained was almost identical to that produced from a solution containing ferric nitrate only (Table 1). Clearly, under the RTDS processing conditions used for these experiments, the Fe^{2+} was rapidly oxidized to Fe^{3+}.

Doping of the iron feed solution with Cr^{3+} salt at a 10:1 iron to chromium ratio yielded a solid powder consisting of hematite and 6-line ferrihydrite after processing at 300°C. No distinct chromium-only phase was detected in the powder collected. Because of significant broadening of the lines in the XRD pattern due to the fine crystallite size in this material, it was not clear whether significant amounts of chromium had been incorporated into the hematite structure.

RTDS processing at 350°C of a feed solution consisting of $Fe(NO_3)_3$ and $Ni(NO_3)_2$ in a 2:1 mole ratio (0.067 M: 0.033 M, respectively) yielded a reddish-brown solid powder product. XRD analysis of the powder indicated the presence of only the hematite phase. No nickel-bearing phase was detected. Addition of 0.5 M urea to the Fe^{3+}/Ni^{2+} solution and processing at 350°C yielded a powder consisting primarily of the nickel ferrite, trevorite ($NiFe_2O_4$), with a smaller concentration of its hydroxide precursor.

Powder generated from a Fe^{3+}/Cu^{2+} salt solution at a 350°C processing temperature consisted of a mixture of hematite and 6-line ferrihydrite. No copper-only phase was detected in the XRD analysis of the precipitated solid. Addition of 0.5 M urea to the Fe^{3+}/Cu^{2+} feed solution and processing at 350°C resulted in precipitation of the copper oxide phase, tenorite (CuO) and a separate hematite phase. XRD results on the settled powder gave no indication of the formation of a ferrite phase similar to that observed in the Fe^{3+}/Ni^{2+} system with the use of urea as a precipitating agent.

SUMMARY

The RTDS process is a viable method for hydrothermally generating ultrafine iron-bearing catalyst powders having crystallite sizes into the nanometer size range. Specific crystalline phases and crystallite sizes of the iron-based powders generated by this method are influenced by the

processing conditions to which the feed solutions are subjected and to the species present in those solutions.

ACKNOWLEDGEMENTS

Pacific Northwest Laboratory (PNL) is operated for the U.S. Department of Energy (DOE) by Battelle Memorial Institute under Contract DE-AC06-76RLO 1830. The work reported here was sponsored by the DOE Office of Fossil Energy and by DOE under the Advanced Processing Technology Initiative at PNL.

REFERENCES

(1) Pradhan, V.R.; Herrick, D.E.; Tierney, J.W.; Wender, I. *Energy Fuels* **1991**, *5*, 712-720.
(2) Suzuki, T.; Yamada, H.; Sears, P.; Watanabe, Y. *Energy Fuels* **1989**, *3*, 707-713.
(3) Matson, D.W.; Linehan, J.C.; Bean, R.M. *Mater. Lett.* **1992**, *14*, 222-226.
(4) Linehan, J.C.; Darab, J.G.; Matson, D.W. "Results of Catalyst Testing Using Iron-Based Catalysts," This proceedings.
(5) Schwertmann, U.; Cornell, R.M. *Iron Oxides in the Laboratory*, Weinheim: New York, 1991.
(6) Huffman, G.P.; Ganguly, B.; Taghiei, M.; Huggins, F.E.; Shah, N. *Preprints, Div. of Fuel Chem., American Chemical Society* **1991**, *36*, 561-569.

TABLE 1
RTDS Powders Produced from 0.1 M $Fe(NO_3)_3$ Solutions

Added Component	RTDS Temp. (°C)	Identified Phase[a]	Crystallite Diameter (nm) by: XRD[b]	TEM[c]	Mossbauer[d]	BET Surface Area (m^2/g)
-----	225	2-line Ferrihydrite[e]	<<10	2-10	---	212
-----	300	Hematite	11	4-10	56% > 8.5	167
-----	400	Hematite	23	20-40	100% > 8.5	—
acetate buffer	225	---	<<10	2-10	100% < 8.5	184
urea	200	—	—	—	—	—
urea	250	6-line Ferrihydrite	<<10	—	—	—
urea	300	6-line Ferrihydrite	<<10	—	—	—

[a]Determined by XRD
[b]Estimates of uncertainties in XRD size results are ± 10% for crystallites in the 10 to 120 nm range.
[c]TEM size estimates are qualitative and based on both bright-field and dark-field observations.
[d]Size distribution about 8.5 nm was based on relative areas of the quadrupole doublet vs. the 6-line hyperfine feature in room temperature spectra.[6]
[e]Two-line ferrihydrite and 6-line ferrihydrite are poorly defined hydrated iron (hydroxy) oxide phases which are distinguished from each other by the number of broad lines present in their XRD patterns.

TABLE 2
Results of Co-Processing Aqueous Ferric
Nitrate Solutions with Other Metal Ions[a] using RTDS

Other Salt	$[Fe^{3+}]:[M]$	Reaction Temperature	Identified Products[b]	Crystallite Diameter[c]
$FeSO_4$	1:1	225°C	50% Hematite, 50% 6-Line Ferrihydrite	37 nm <<10 nm
$FeSO_4$	1:1	300°C	90% Hematite, 10% 6-Line Ferrihydrite	36 nm <<10 nm
$FeSO_4$	1:1	400°C	100% Hematite	32 nm
$Cr(NO_3)_3$	10:1	300°C	40% Hematite, 60% 6-Line Ferrihydrite	12 nm << 10 nm
$Cu(NO_3)_2$	2:1	350°C	70% Hematite, 30% 6-Line Ferrihydrite	11 nm <<10 nm
$Cu(NO_3)_2$ + Urea	2:1	350°C	30% Hematite, 70% Tenorite (CuO)	11 nm 22 nm
$Ni(NO_3)_2$	2:1	350°C	100% Hematite	15 nm
$Ni(NO_3)_2$ + Urea	2:1	350°C	80% Trevorite ($NiFe_2O_4$), 20% δ-$(Fe_{0.67}Ni_{0.33})OOH$	8.5 nm <<10 nm
$Ni(NO_3)_2$ + Urea	2:1	400°C	90% Trevorite ($NiFe_2O_4$), 10% δ-$(Fe_{0.67}Ni_{0.33})OOH$	7.4 nm <<10 nm

[a]Total cation concentration 0.1 M for all starting solutions [b]Determined by XRD analysis
[c]By XRD line broadening

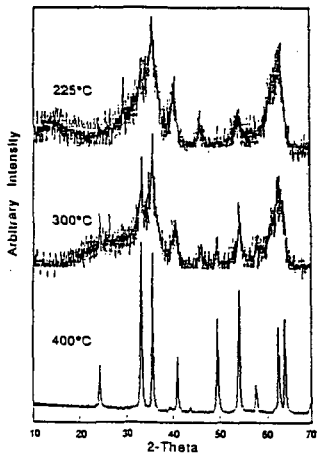

Figure 1. Variations in XRD patterns of RTDS-generated iron oxide powders as a function of increasing RTDS processing temperature.

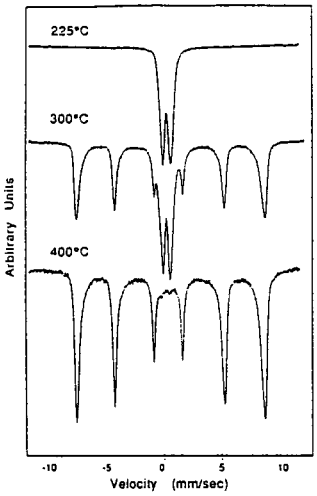

Figure 2. Variations in Mossbauer spectra of RTDS-generated iron oxide powders as a function of increasing RTDS processing temperature.

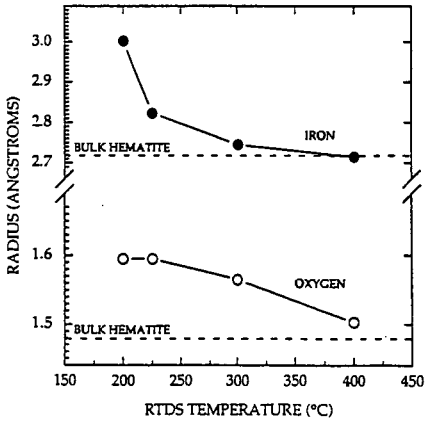

Figure 3. Plot of iron nearest neighbor radii determined from the iron K-edge EXAFS spectra of RTDS powders produced from 0.1 M ferric nitrate solutions

Synthesis and Characterization of Fe and FeS_2 (Pyrite) Catalyst Particles in Inverse Micelles*

A. Martino, J.P. Wilcoxon, A.P. Sylwester, J.S. Kawola
Fuel Science Division, 6211
Sandia National Laboratories
Albuquerque, NM 87185

Keywords: Inverse micelles; Nanophase clusters; Coal liquefaction catalysts

Introduction

Surfactant molecules possess two distinct moieties: a hydrophilic head group and a hydrophobic tail group. Because of the dual nature of surfactant molecules, they self-assemble in various solvents. In many two component systems of surfactant and oil, surfactants aggregate to form inverse micelles. Here, the hydrophilic head groups shield themselves by forming a polar core, and the hydrophobic tail groups are free to move about in the surrounding oleic phase. In three component microemulsion systems of water, oil, and surfactant, water is solubilized within the inverse micelle structure if the water concentration remains low. The solution takes on the structure of water droplets approximately 10-100Å in diameter dispersed in the oleic solvent with surfactant forming the boundary between the two components.

In structured solutions such as inverse micellar and oil-rich microemulsion solutions, polar chemical reactants can be compartmentalized in the interior of the surfactant aggregates. If a chemical reaction sequence is initiated, the surfactant interface provides a spatial constraint on the reaction volume. The surfactant aggregates act as micro-reactors. Metal alkoxide reactions [1], the formation of metal and semiconductor clusters [2-5], and the formation of polymer particles [6] are examples of chemical processes which have been carried out in structured surfactant solutions.

We have studied the formation of iron based clusters in inverse micelles and their use as catalysts in coal liquefaction reactions. Iron salts are solubilized within the polar interior of inverse micelles. The addition of an organic based reducing agent or water based sulfiding agent initiates respectively a chemical reduction or an exchange/replacement reaction. The inverse micelle structure acts as a reaction media and limits the final size of the particles. Particle formation is also dependent upon the particle nucleation and growth process. The initial micelle size, the nucleation and growth process, and ultimately the size of the particles is controlled by adjusting a few experimental parameters.

In order to illustrate the effects of various experimental conditions on the final particle size, we have studied a model system. CdS formation is well understood. We report the use of small angle neutron scattering, UV-visible spectrophotometry, and electron microscopy to characterize the inverse micelle solutions, the particle size, and particle elemental composition. Analogous results are observed in the formation of Fe and FeS_2 (pyrite). Finally, we report the use of the iron based clusters as catalysts in batch coal liquefaction reactions.

Experimental

Alkanes of increasing hydrophobicity from hexane to hexadecane, cyclohexane, and toluene were purchased from Aldrich at 99.9+% purity. Surfactants used included didodecyldimethylammonium bromide (DDAB) from Kodak, butyl-ethylene glycol n-dodecyl ether ($C_{12}E_4$) from Nikkol, and POE (6) nonylphenol from Chem Services. Metal salts used included cadmium chloride, iron(II) chloride tetrahydrate, and iron(III) chloride hexahydrate from Aldrich. Lithium borohydride in tetrahydrofuran (1M) was purchased from Aldrich. Lithium sulfide was

* This work is supported by the U.S. Department of Energy at Sandia National Laboratories under contract DE-AC04-76DP00789.

purchased from Aldrich and prepared in a 1M solution in de-ionized, distilled water. Otherwise, all chemicals were used as delivered.

Stock solutions of 10 wt. % surfactant are prepared in various organic solvents to produce the inverse micelle solutions. The iron salts are added directly to prepare 0.001-0.01M solutions, and are mixed overnight on a stirring plate to assure complete solubilization. Concentrated aqueous cadmium chloride solutions are mixed with the stock inverse micelles solutions to prepare 0.0005-0.01M cadmium chloride microemulsions. To reduce the iron salts, the concentrated $LiBH_4$/THF solution is injected into the inverse micelle solutions under rapid stirring. To sulfide the iron and cadmium salts, the Li_2S/H_2O solution is injected into the inverse micelle or microemulsion solutions under rapid stirring. The reaction is carried out and the final product is stored under dry, oxygen-free conditions. The reducing agent or sulfiding agent is added in an excess molar concentration to favor the formation of the surfactant stabilized sols.

The inverse micelle and cluster solutions are studied by small angle neutron scattering (SANS), UV-visible spectrophotometry, and electron microscopy (TEM). SANS is carried out at the *Low-Q Diffractometer* at the *Los Alamos Neutron Scattering Center*. Deuterated organic solvents are used. The inverse micelle radius of gyration is determined by Guinier analysis of the scattering curve [7]: $I = N \exp(-q^2R_g^2/3)$, where N is a proportionality constant, q is the scattering vector, and R_g is the radius of gyration of the inverse micelles. UV-visible spectrophotometry of the particle solutions is completed *in-situ* with a Hewlett Packard 8452A diode array spectrophotometer. Relative size and characterization of the particles is achieved through analysis of the plasmon resonances observed in metal particles and the band gap structure observed in semiconductors. Finally, TEM using a Joel 1200EX sizes the particles and selected area electron diffraction aids in the particle characterization.

Coal liquefaction of DECS-17, Blind Canyon coal is completed in a stainless steel micro-batch reactor at 400°C, a cold H_2 pressure of 800 psi, and a reaction time of 30 minutes. Hexahydropyrene (H_6Py) is used as the hydrogen donor solvent. Thermal conditions are selected to give moderate conversion of coal to relatively low molecular weight organic material. Reaction analysis consists of extracting products with THF and heptane (C7) in two separate stages, and the products are separated into categories depending on their solubility for the solvents. Insoluble organic matter (IOM) is neither soluble in THF or C7. All soluble organic matter is extracted by THF (THF solubles), and the low molecular weight fraction of this material is extracted by C7 (C7 solubles). This latter fraction of product represents potentially usable oils and gases. Product gas analysis was not completed. A description of the coal liquefaction process is detailed elsewhere [8]. The iron based catalysts were tested *in-situ* or as powders and were added to the micro-batch reactors directly.

Results

Small angle neutron scattering results indicate that inverse micelles of $C_{12}E_4$ in octane and dodecane increase in size with the addition of water (Figure 1). The effect of water addition is more drastic in dodecane than in octane. Also, the inverse micelle size increases as the oil hydrophobicity increases (i.e. $C_{12}E_4$/dodecane inverse micelles are roughly 12% bigger than $C_{12}E_4$/octane inverse micelles).

Transmission electron microscopy of FeS_2 formed in $C_{12}E_5$/octane inverse micelles show ~ 10Å radius particles ($C_{12}E_5$ is a slightly more hydrophilic analog of $C_{12}E_4$). Initial concentration of the iron salt was 0.001M. The particles show no signs of aggregation and are highly dispersed, spherical, and monodisperse on the TEM grid (Figure 2). TEM results indicate Fe^0 particles formed in DDAB/toluene (initial iron salt concentration = 0.001M) are ~ 12Å in radius. In addition, lattice fringe imaging indicates that the Fe^0 colloids exist in the high temperature fcc Fe(γ) structure. Finally, CdS particles formed in $C_{12}E_5$/octane inverse micelles (initial cadmium salt concentration = 0.0005M) are ~14Å in radius as determined by TEM.

The electronic spectra of CdS semiconductor particles is well known [3]. An absorbance shoulder is observed in the visible wavelength range due to the formation of an electron-hole pair across the semiconductor band gap. This spectra is reproduced by UV-visible spectrophotometry in

the CdS particles produced in inverse micelles (Figure 3). Increasing water concentration in the microemulsion solution causes a red shift in the onset of visible absorbance and a red shift in the absorbance maxima. The maxima occurs just before the large solvent absorbance shoulder. The electronic spectra is not effected by the solvent. The absorbance onset and maxima are nearly identical in octane and hexadecane.

The electronic spectra of FeS_2 particles is also dependent on water concentration in the microemulsion solutions (Figure 4). The spectra is highlighted by several absorbance maxima which red shift as the water concentration increases in the microemulsion mixtures. The behavior of the FeS_2 electron spectra is analogous to the behavior of the CdS electronic spectra as a function of water content.

As further characterization of the FeS_2 particles, electron diffraction from a selected area on the microscope grid produces a ring pattern consistent with the FeS_2 pyrite structure (Figure 5).

Finally, the Fe and FeS_2 particles were tested as catalysts in coal liquefaction reactions. Results are shown in Table 1. Solvent dispersed Fe or FeS_2 catalysts show equal or lower conversion to organic products compared to the thermal (no catalyst) reactions. The liquid catalysts show high amounts of insoluble organic matter. Fe catalyst added as a powder shows equal conversion to organic products compared to the thermal runs. FeS_2 catalyst added as a powder shows lower overall conversion to organic products, but a higher conversion to low molecular weight products. Importantly, the catalyst selectivity for the production of low molecular weight products is greatly increased.

Discussion

Colloid formation in the reduction and exchange/replacement processes proceed, respectively, via the following chemical reactions: $Fe^{2+} + 2H^- \text{----> } Fe(colloids) + H_2$ and $Fe^{2+} + S_2^{2-} \text{----> } FeS_2(colloids)$. The inverse micelles act as reaction vessels and mediate the nucleation and growth of the particles. The surfactant stabilizes the colloids and prevents flocculation and precipitation. Nevertheless, colloid stability is dependent on the high reactivity of the particles. It is necessary to use excess reactants in order to push the chemical reactions to the right and favor the formation of the colloids. In the case of the sulfiding reaction, water in the microemulsion mixtures favor the decomposition of the colloids into their respective ions. This is observed by the disappearance of the characteristic absorbance spectra of CdS and FeS_2. The presence of water in the reduction reaction of iron salts may change the chemistry all together and actually lead to the formation of iron borides and oxides. Oxidation of the iron clusters is visible to the naked eye, and CdS colloids photodegrade in the presence of oxygen ($CdS + 2O_2 \text{----> } Cd^{2+} + SO_4^{2-}$). The oxidation of both FeS_2 and CdS can be witnessed by the disappearance of their respective absorbance spectra.

Particle size control in the inverse micelle mediated synthesis of clusters is complex. It is reasonable to expect that the size of the initial inverse micelle will limit the final particle size. New particles will nucleate before existing particles grow large enough to disrupt the micelle structure. The nucleation and growth process is also governed by such variables as initial salt concentration, solution viscosity, and temperature. Any variable which increases the effective diffusion rate of the reacting ions will favor growth over nucleation and lead to larger particles.

We have attempted to elucidate the most relevant variables in the control of the final particle size. The electronic spectra of the semiconductor CdS provides us with the most facile method to determine relative particle size. The band gap of semiconductor particles increases with decreasing particle size due to quantum confinement of the charge carriers. Increasing particle size will cause a red shift in the absorbance spectra of fine particles [2]. The electronic spectra of CdS particles clearly show this behavior. Figure 1 shows that the size of inverse micelles is strongly dependent on water content and only weakly dependent on the hydrophobicity of the oil. The electronic spectra of particles synthesized in the same inverse micelles show a distinct red shift with increasing water content (Figure 3). There is little shift in the electronic spectra as the solvent changes from octane to hexadecane despite a six-fold change in solution viscosity. Clearly, the changing size of the initial inverse micelle plays a larger role in the final particle size than does ionic diffusion of reacting species as controlled by solution viscosity.

The electronic spectra of FeS_2 is dependent on the water content of the reacting microemulsion system (Figure 4). If we assume that the particles grow with increasing water content, then we can infer that the electronic spectra is size dependent for the FeS_2 particles. This is consistent with the formation of pyritic FeS_2 which is a semiconductor. The ring pattern of the selected area electron diffraction is consistent with the structure of pyritic FeS_2 and corroborates the electronic spectral data.

Iron sulfide has been studied extensively as a coal liquefaction catalyst. It is believed that pyrrhotite ($Fe_{1-x}S$) is the active form of the iron catalyst under liquefaction conditions [9], and that pyrite is reduced to pyrrhotite under liquefaction conditions [10]. We have attempted to use our Fe and FeS_2(pyrite) particles as coal liquefaction catalysts. Wetting of Blind Canyon with our highly dispersed particle solutions causes coal aggregation and poor mixing. Aggregated coal which does not participate in the liquefaction process appears in the product as insoluble organic matter. Fe powder shows no improvement over thermal reactions perhaps indicating a need to sulfide the catalyst. FeS_2 (pyrite) powder however shows good selectivity towards the production of low molecular weight products at the same time that the insoluble organic matter content remained high. We infer that our catalyst shows high selectivity for reducing polar functionalities within Blind Canyon. Further studies of product quality are in progress.

Conclusions

Monodispersed, nanometer sized particles of Fe, FeS_2 (pyrite), and CdS are synthesized in inverse micelle solutions. Oil rich inverse micelle solutions are characterized by a structure in which surfactant interfaces protect a polar core from the oleic phase. Iron or cadmium salts are taken up in the polar core, and the clusters are formed upon chemical reduction or chemical exchange/replacement reactions. The inverse micelles provide size and geometric constraints on the growth of the clusters and stabilize the highly dispersed sols. The effect of initial micelle size as controlled by water content influences the final particle size more than solution viscosity which regulates the nucleation and growth of the particles. We have used the size dependent electronic spectra and selected area electron diffraction to characterize the formation of pyritic FeS_2. Finally, the iron based clusters were tested as catalysts in a coal liquefaction process. While liquids wet the coal and prevent adequate mixing, FeS_2 powder selectively increases conversion to low molecular weight oils.

References

1. J.H. Jean and T.A. Ring, *Colloids and Surfaces*, **29**, 273, 1988.
2. M.L. Steigerwald and L.E. Brus, *Annu. Rev. Mater. Sci.*, **19**, 471, 1989.
3. B.H. Robinson, T.F. Towey, S. Zourab, A. Visser, and A. van Hoek, *Colloids and Surfaces* **61**, 175, 1991.
4. M. Boutonnet, J. Kizling, R. Touroude, G. Maire, and P. Stenius, *Catalysis Letters*, **9**, 347, 1991.
5. J.P. Wilcoxon and R.L. Williamson, *Mat. Res. Soc. Symp. Proc.*, **177**, 269, 1990.
6. L.M. Gan and C.H. Chew, *J. Dispersion Science and Technology*, **4**, 291, 1983.
7. G. Porod, Small Angle X-ray Scattering, Eds. O. Glatter and O. Kratky, pp. 24, Academic Press, 1983.
8. F.V. Stohl, Preprints of Papers Presented at the 205th ACS National Meeting, Denver, CO, 3/28-4/2/93, American Chemical Society, Division of Fuel Chemistry.
9. R.M. Davidson, *IEA Coal Research*, pp. 100, 1983.
10. T. Kotanigawa, S. Yokoyama, M. Yamamoto, and Y. Maekawa, *Fuel*, **66**, 1452, 1987.

TABLE 1. Micro-batch liquefaction results of Blind-Canyon, DECS-17 coal. Conditions: T = 400°C, P = 800 psi cold H_2, t = 30 min, hexahydropyrene solvent, 2-5 wt. % catalyst. Gas analysis is not included in these results.

CATALYST	% IOM	% THF SOLS/C7 INSOLS	% C7 SOLS
thermal, average	9.9	58.0	30.1
Fe, *in-situ*	66.5	13.8	8.9
Fe, powder	6.0	60.9	30.5
Fe, surfactant extracted liquid	50.0	27.3	22.7
FeS_2, *in-situ*	64.7	34.3	1.0
FeS_2, powder	17.0	33.9	44.4
FeS_2, surfactant extracted liquid	9.8	57.3	28.7

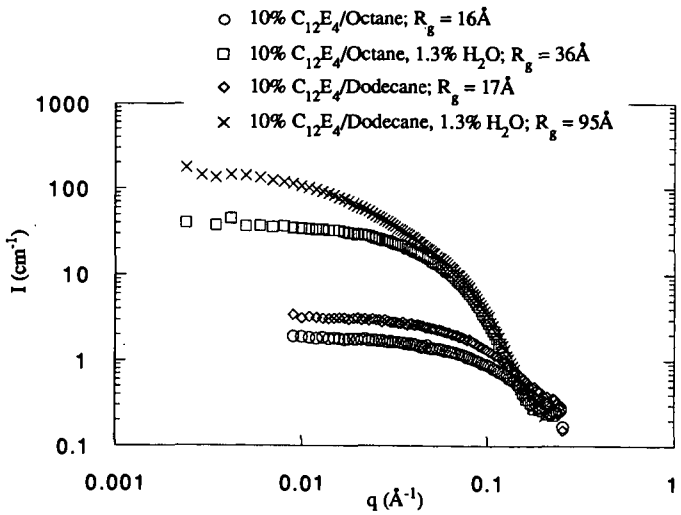

Figure 1. Small angle neutron scattering of inverse micelles. The inverse micelles grow as water concentration increases and as the oil alkane chain number increases.

Figure 2. TEM of FeS_2 (pyrite) clusters. The cluster radius is ~ 10Å. The particles are highly dispersed and monodispersed. TEM's of Fe clusters show ~ 12Å radius particles and CdS clusters are ~ 14Å in radius.

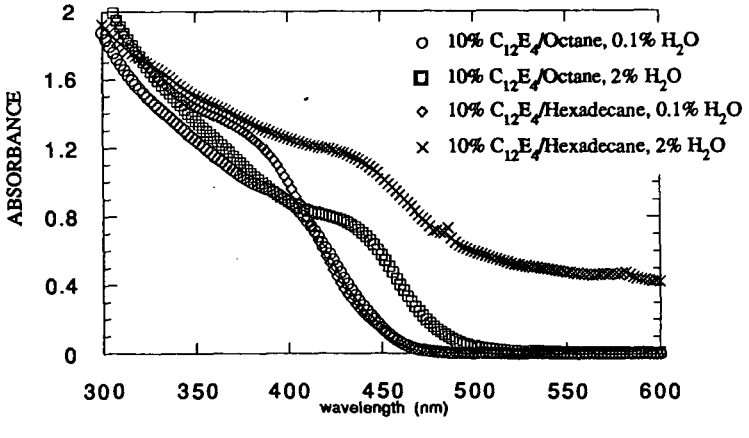

Figure 3. Electronic spectra of CdS clusters as a function of water content in two oil systems. As water content increases the absorbance maxima and onset red shift indicating an increase in the particle radius.

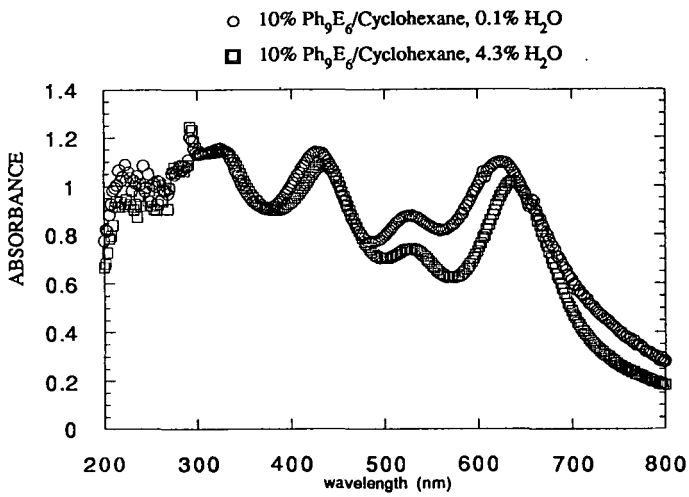

Figure 4. The electronic spectra of FeS_2 shows a red shift as water content increases. The size dependent band gap shift is characteristic of the semiconductor nature of pyrite.

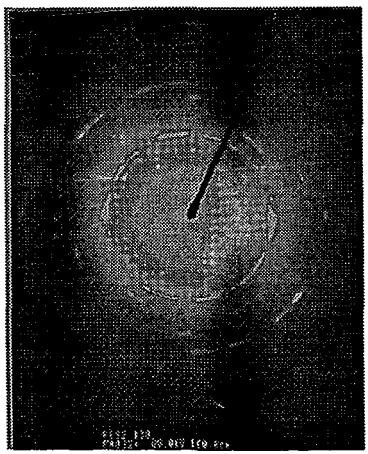

Figure 5. Selected area electron diffraction of FeS_2 shows a ring pattern consistent with the structure of pyrite.

REVERSE MICELLE SYNTHESIS OF NANOSCALE METAL CONTAINING CATALYSTS

John G. Darab, John L. Fulton and John C. Linehan
Pacific Northwest Laboratory[1], Richland, Washington 99352

KEYWORDS: catalyst synthesis, EXAFS, microemulsion

INTRODUCTION

The need for morphological control during the synthesis of catalyst precursor powders is generally accepted to be important. In the liquefaction of coal, for example, iron-bearing catalyst precursor particles containing individual crystallites with diameters in the 1-100 nanometer range are believed to achieve good dispersion through out the coal-solvent slurry during liquefaction runs and to undergo chemical transformations to catalytically active iron sulfide phases[2].

The production of the nanoscale powders described here employs the confining spherical microdomains comprising the aqueous phase of a modified reverse micelle (MRM) microemulsion system as nanoscale reaction vessels in which polymerization, electrochemical reduction and precipitation of solvated salts can occur. Figure 1 shows a schematic illustration of a typical reverse micelle for the system studied here. The goal is to take advantage of the confining nature of micelles to kinetically hinder transformation processes which readily occur in bulk aqueous solution in order to control the morphology and phase of the resulting powder. A micellar approach to producing nanoscale particles has already been used on a variety of semiconductor, metal and ceramic systems[3]. The synthetic approach described here is unique, however, in that a much greater yield of powder can be obtained compared to the conventional reverse micelle systems (approximately 10 g/l for the MRM system vs 0.5 g/l for traditional reverse micelle systems).

We have prepared a variety of metal, alloy, and metal- and mixed metal-oxide nanoscale powders from appropriate MRM systems. Examples of nanoscale powders produced include Co, Mo-Co, Ni_3Fe, Ni, and various oxides and oxyhydroxides of iron. Here, we discuss the preparation and characterization of nickel metal (with a nickel oxide surface layer) and iron oxyhydroxide MRM nanoscale powders. We have used extended x-ray absorption fine structure (EXAFS) spectroscopy to study the chemical polymerization process *in situ*, x-ray diffraction (XRD), scanning and transmission electron microcroscopies (SEM and TEM), elemental analysis and structural modelling to characterize the nanoscale powders produced. The catalytic activity of these powders is currently being studied.

EXPERIMENTAL SECTION

Powder Precursor Salts. Ammonium ferric sulfate dodecahydrate (Fisher) and nickel sulfate hexahydrate (Fisher) were used as-received as precursor salts for iron- and nickel-bearing powders respectively.

Preparation of the Microemulsions (MRMs). In a 2.0-l Erlenmeyer flask 12-gm sodium dodecyl sulfate (SDS) and 80-ml of the 1.0 M aqueous metal salt solution of interest were mixed. To this slurry was added 1-l 0.12 M sodium bis(2-ethylhexyl) sulfosuccinate sodium salt (aerosol-OT or AOT) in isooctane. After rigorous stirring and gentle warming for approximately thirty minutes, an optically transparent microemulsion resulted. Two similar microemulsions were prepared using either 1.0 M aqueous sodium hydroxide or sodium borohydride in place of the metal salt containing solution. Microemulsions were used immediately after preparation.

Preparation of Powders. The nickel metal powder was prepared by adding sodium borohydride MRM to the nickel sulfate MRM slowly with constant stirring. Iron oxyhydroxide powder was similarly prepared by adding sodium hydroxide MRM to the ammonium ferric sulfate MRM. In both cases, after about ten minutes particle formation became apparent as the resulting microemulsion began to change color (from green to black for nickel metal formation, and from yellow/orange to red for iron oxyhydroxide formation) and scatter light. The suspension was then transferred to 500-ml nalgene centrifuge tubes and centrifuged at 6000 RPM for ten minutes. The remaining liquid was decanted off. The compacted powder at the bottom of the centrifuge tubes was then washed and centrifuged in isooctane three times. This was followed by three washings/centrifugings in each of methylene chloride and finally water. Water acidified with HNO_3 was used to wash the nickel powders in order to remove salt biproducts. The wet powders were dried under vacuum at 60°C for 24 hours, then ground in a mortar and pestle.

***In Situ* Study of Particle Formation.** The sodium hydroxide MRM was added to the ammonium ferric sulfate MRM stepwise. After each addition, iron K-edge EXAFS spectra were obtained (see below) from the resulting MRM. Sodium hydroxide MRM was added until the system became translucent as a result of nucleation and precipitation of iron-bearing particles.

EXAFS Measurements and Analysis. Iron K-edge EXAFS spectra were obtained on beam line X19A at the National Synchrotron Light Source, Brookhaven National Laboratory. The data were recorded in a transmission mode using either powders thinly distributed onto cellophane tape, or liquids or suspensions contained in a specially prepared sample cell. For each sample, between three and fifteen scans were recorded and averaged together. Standard EXAFS data analyses were applied to the averaged data to obtain a radial distribution function (RDF)[4]

Additional Characterization of Powders. Scanning and transmission electron microscopies (SEM and TEM) and powder x-ray diffraction (XRD) were performed on the as-prepared powders. A portion of the as-prepared iron oxyhydroxide powder was sent out to a commercial analytical lab (Desert Analytical, Tuscon, Arizona) to be analyzed for Fe, C, S, Na and N.

RESULTS AND DISCUSSION

Nickel Powder. Figure 2 shows an SEM micrograph of the as-prepared MRM nickel powder, indicating that the powder consists of irregularly shaped, sponge-like particles with diameters of 1-10 microns. The particles appear to be aggregates of extremely fine crystallites. XRD analysis confirms the formation of phase-pure nickel metal with an average crystallite size of 12-nm. No oxide phases were detected by XRD. However, energy dispersive spectroscopy (EDS) performed in the scanning electron microscope did detect the presence of oxygen, presumable in the form of a thin oxide layer on the surface of the nickel metal particles. Elemental and BET surface area analyses have not yet been performed on this powder.

The sponge-like morphology of the nanoscale MRM nickel metal powder, which presumably has a high surface area, makes it ideal as a highly dispersable catalyst for various industrial processes. As with most metal surfaces, a ubiquitous metal oxide layer is present on the surface of these nanoscale nickel powders; however, the total oxide content must be less than several weight percent due to the fact that no oxide phases are detected via XRD.

Iron Oxyhydroxide Powder. The dried powder consisted predominantly of irregularly shaped particles with diameters of 1-10 microns. TEM analysis on individual particles reveals no resolvable microstructural features, indicating that the particles are either amorphous or agglomerates of nanometer size crystallites. XRD analysis indicates that the powder has the same diffraction pattern as an iron oxyhydroxide phase typically referred to as two-line ferrihydrite[5]. The elemental analysis of the as-prepared powder shows that it contains 45.62 wt% Fe, 11.62 wt% C, 2.56 wt% S, 0.17 wt% Na and 0.12 wt% N. EDS analysis on the powder confirmed the presence of carbon and sulfur. BET analysis indicates that the surface area of the as-prepared powder is greater than 200-m^2/gm.

Aqueous Chemistry of Iron(III) Species. Most 1 M aqueous iron(III) salts in bulk acidic non-complexing solutions contain octahedrally coordinated iron(III)-aquo monomeric complexes, $[Fe(H_2O)_6]^{3+}$, in equilibrium with dimeric $[Fe_2(H_2O)_8(OH)_2]^{4+}$ and trimeric $[Fe_3(H_2O)_9(OH)_4]^{5+}$ species[6-8]. The addition of base (e.g. NH_3, NaOH, etc.) to the non-complexing aqueous iron(III) salt solution causes polymerization of the monomeric, dimeric and cyclic trimeric species. In general, polymerization at ambient temperatures occurs via deprotonation of one or two aquo ligands and subsequent olation which forms predominantly edge sharing linkages[6,7]. Livage *et al.*[7] discuss the formation of cyclic trimers via the olation of hydrolyzed monomers with dimers. The addition of another monomer yields a planar tetramer. Further olation between tetramers yields double straight-chain polymers.

Under appropriate pH conditions, sulfate ligands can chelate and remain stongly bound to the iron(III) cation even after particle precipitation, giving rise to sulfated iron oxyhydroxides with disordered polymer chains (e.g. kinked- or straight-single chain polymers)[5,7]. Since the synthetic technique employed here uses sulfate salts, and sulfate and sulfonate containing surfactants, these issues become critical. Chemical and structural analyses of the resulting MRM powders will be used to identify the role of sulfo ligands in the powder preparation process.

The elemental analysis of the as-prepared iron oxyhydroxide powder indicates that an appreciable amount of sulfur has been incorporated into the powder product (iron-to-sulfur molar ratio equals 10.2). Since the elemental analysis also indicates that the molar ratio of carbon-to-sulfur is 12.1 and very little sodium is incorporated into the as-prepared powder, the complexation of the iron(III) cation by dodecyl sulfate groups from the SDS seems most probable. Whether these sulfate groups actually take part in the polymerization reactions occurring in the aqueous cores of the reverse micelles or become associated with the particle surface after precipitation is still uncertain.

Structural Modelling of the Iron-Bearing Powder. Extracting the average number of nearest neighbors from an EXAFS spectrum, especially from those obtained from highly disordered systems (i.e., solutions, suspensions, and amorphous materials) and/or nanometer size grains like those being currently studied, often yields values which are suspect due to structural disorder and Debye-Waller damping[9]. Thus, only comparisons between the various nearest neighbor distances determined from the EXAFS spectra of bulk standards and of *in situ* studies of the MRM system will be considered as valid criteria in trying to elucidate the structure of the iron-bearing particles being formed.

There are primarily seven basic oxide and oxyhydroxide phases of iron which could form under the conditions used in this work: goethite (α-FeOOH), akaganeite (β-FeOOH), lepidocrocite (γ-FeOOH), feroxyhyte (δ'-FeOOH), two-line ferrihydrite (unknown structural formula), six-line ferrihydrite (see below) and hematite (α-Fe_2O_3)[5].

Goethite, akaganeite and lepidocrocite are all composed of different arrangements of double straight polymer chains connected via corner or edge sharing bonds. The primary structural order in all of these phases, i.e. the bonding in the double straight chains, are identical[8] and thus yield identical oxygen and iron first nearest neighbor shell radii.

In contrast, feroxyhyte, six-line ferrihydrite and hematite are built up from polymer chains and sheets containing a combination of edge, face and corner sharing linkages, and are thus distinguished from the double straight chain-based phases at the primary structural level. These three phases are all structurally similar in that two layers of the edge, face and corner sharing polymer sheets make up the feroxyhyte structure, while that of the six-line ferrihydrite contains four layers, and that of hematite contains six layers.

In terms of the oxygen and iron first nearest neighbor radii determined using EXAFS then, one can discuss whether the primary structural order of the MRM derived powder is goethite-like or hematite-like. Figure 3 shows the oxygen and iron first nearest neighbor radii determined from the EXAFS RDFs plotted versus the [OH]/[Fe] ratio. Note that as the [OH]/[Fe] ratio increases, the iron first nearest neighbor distance systematically decreases and approaches those representative of bulk phases. This indicates that the iron oxyhydroxide polymers, which may be incorporating some sulfate groups, are becoming larger and more highly condensed. The oxygen nearest neighbor distance initially increases with increasing [OH]/[Fe] ratio but then decreases and eventually approaches those representative of bulk phases. The reason for this behavior in the oxygen nearest neighbor distance is uncertain. After precipitation occurs ([OH]/[Fe] = 2.03) and the resulting powder is washed and dried, the oxygen and iron

first nearest neighbor distances become identical to those found in the goethite phase. We thus conclude that the particles formed in the MRM system are goethite-like in structure.

The XRD pattern for the proto-goethite MRM powder, however, is not representative of bulk goethite but of two-line ferrihydrite, the structure of which is still not well understood. Although two-line ferrihydrite is structurally disordered[5], its primary structural has been previously investigated using EXAFS[10,11] and has been shown to be similar to that of goethite[12]. We suggest that the iron bearing powder being produced by the MRM process indeed has a goethite-like primary structure but lacks the necessary long-range order observed in bulk goethite, indicating that the particles are extremely small and/or disordered and are most likely in an early stage of development. At such early developmental stages, goethite, akaganeite and lepidocrocite are all structurally identical, i.e., double or disordered double straight polymer chains. Akaganeite and lepidocrocite generally do not form under the conditions used in this work; therefore, as a matter of convenience we have labeled this phase of the as-prepared MRM powder as "proto-goethite".

This proto-goethite structure, which may be related to two-line ferrihydrite, consists of double straight chains or disordered double straight chains with iron and/or oxygen vacancies linked together to form a secondary structure having, at best, limited order. The suggestion that the double straight chains are possibly disordered should not be surprising as it was previously noted that the presence of sulfate anions in the aqueous cores of the reverse micelles could become incorporated into the growing polymer, producing such disordered structures.

SUMMARY

Using a modified reverse micelle process, tens-of-gram per liter quantities of micron sized particles of nanoscale nickel metal and iron oxyhydroxide were produced. The as-prepared nickel metal particles were found to consist of agglomerates of nanometer sized crystallites of nickel having a surface oxide layer. The as-prepared iron oxyhydroxide particles were determined to be either amorphous or agglomerates of nanometer sized crystallites having a structure which is proto-typical to that of goethite.

ACKNOWLEDGEMENTS

This work was supported by the U.S. Department of Energy, Office of Fossil Energy under contract DE-AC06-76RLO 1830 and the Advanced Processing and Technology Initiative.

The assistance of Y. Ma in the collection and analysis of the EXAFS data was most appreciated.

REFERENCES

1. Pacific Northwest Laboratory is operated for the United States Department of Energy by the Battelle Memorial Institute.
2. (a) Pradhan, V.R.; Tierney, J.W.; Wender, I.; Huffmann, G.P. *Energy & Fuels* **1991**, *5*, 497. (b) Pradhan, V.R.; Herrick, D.E.; Tierney, J.W.; Wender, I. *Energy & Fuels* **1991**, *5*, 712.
3. Steigerwald, M.L.; Brus, L.E. in *Structure and Reactivity in Reverse Micelles*; Pileni, M.P., ed.; Elsevier: New York, 1989; pp. 189-220.
4. Stern, E.A.; Heald, S. in *Handbook of Synchrotron Radiation*; Eastman, D.E., Farge, Y., Koch, E.E., eds.; North Holland: Amsterdam, 1980.
5. Schertmann, U.; Cornell, R.M. *Iron Oxides in the Laboratory*; VCH: New York, 1991.
6. Flynn, C.M. *Chem. Rev.* **1984**, *84*, 31.
7. Livage, J.; Henry, M.; Sanchez, C. *Prog. Solid State Chem.* **1988**, *18*, 259.
8. Baes, C.F.; Mesmer, R.E. *The Hydrolysis of Cations*; John Wiley and Sons: New York, 1976; pp. 226-237.
9. Lee, P.A.; Citrin, P.H.; Eisenberger, P.; Kincaid, B.M. *Reviews of Modern Physics* **1981**, *53*, 759.
10. Charlet, L.; Manceau, A.A. *J. Coll. Int. Sci.* **1992**, *148*, 443.
11. Combes, J.M.; Manceau, A.; Calas, G.; Bottero, J.Y. *Geochim. Cosmochim. Acta* **1989**, *53*, 583.
12. Manceau, A.; Combes, J.M. *Phys. Chem. Miner.* **1988**, 283.

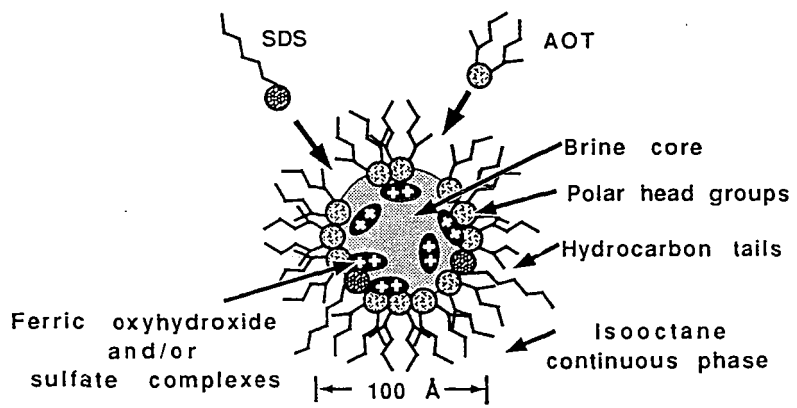

Figure 1. Schematic illustration of a typical reverse micelle for the system studied here.

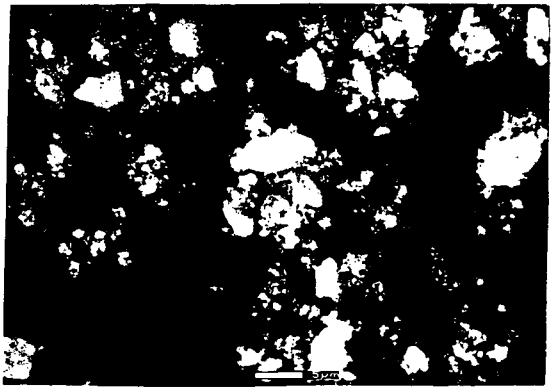

Figure 2. Scanning electron micrograph of the MRM derived nickel metal powder.

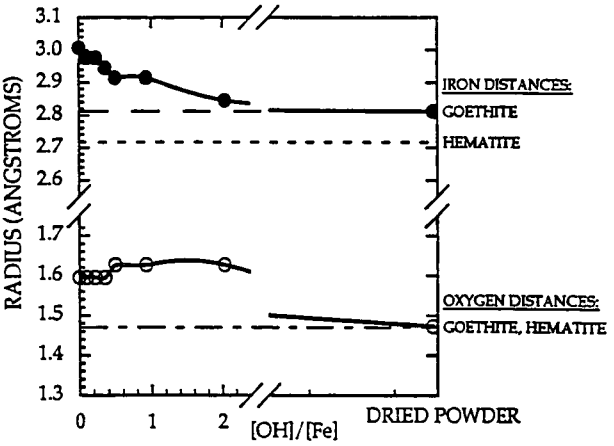

Figure 3. Oxygen and iron first nearest neighbor distances determined from the iron K-edge EXAFS of the ammonium ferric sulfate/ sodium hydroxide MRM microemuslion mixture for various [OH]/[Fe] ratios. Also indicated are the nearest neighbor distances determined for bulk goethite and hematite.

Influence of Nanoscale $Fe_{(1-x)}S$ Particles on Coal Liquefaction

G T Hager, X X Bi, P. C. Eklund, F. J. Derbyshire
Center for Applied Energy Research
University of Kentucky, Lexington,KY 40511

ABSTRACT

It has been shown that during the process of coal liquefaction, iron based catalyst precursors transform to pyrrhotite in the presence of sufficient sulfur. Due to this transformation, the activity of the catalyst initially added relative to the transformed catalyst is not known. In an attempt to address this question, the activity of nanoscale particles of pyrrhotite ($Fe_{1-x}S$), generated by a laser pyrolysis technique, is being studied for the direct liquefaction of a subbituminous coal. Their activity is being compared to that of a similarly prepared iron carbide that is sulfided in situ. The particles produced by this technique have a similar size range and distribution. Comparative studies of the changes in phase and particle size of the catalysts during coal liquefaction experiments are determined by XRD and Mössbauer spectroscopy.

INTRODUCTION

The utility of iron based coal liquefaction catalysts has been known for almost a century. The basis for their use is a combination of moderate activity and relatively low cost, compared to more active catalysts such as Mo, Ti, Ni, etc. A "red mud" iron oxide catalyst precursor was first used in commercial coal liquefaction. It was found that the addition of sulfur with the iron oxide precursor improved the processing of low sulfur coals.[1] Since then, numerous studies have examined different iron phases such as oxides, sulfides, carbides, and organometallic compounds as catalyst precursors. In most of these studies the addition of a source of sulfur has been shown to increase the catalyst activity and selectivity.

Three methods are generally used to introduce the catalyst to the coal. The first is the

physical mixing of a finely divided solid catalyst into the coal feed slurry. This is relatively straightforward and has been used extensively. The second is the addition of an oil-soluble catalyst precursor, such as iron pentacarbonyl, to the coal feed slurry. This method allows almost infinite initial dispersion of the iron. The third method is the addition of the iron to the coal itself, using either an ion exchange technique or by precipitation of a water soluble iron compound within the coal matrix. The former method can only be applied to low rank coals.

Regardless of the method of addition or the precursor composition, in the presence of sulfur the final form of the iron is generally pyrrhotite. Many studies propose that pyrrhotite ($Fe_{1-x}S$)[2,3,4,10] is the active form of iron based catalysts. Indeed, pyrrhotite is the thermodynamically favored phase under liquefaction conditions in the presence of sufficient sulfur. Research has shown that a variety of iron based precursors including oxides[10], sulfides[5,6], carbides[13], and carbonyls[2,3,9] are transformed to pyrrhotite during coal liquefaction.

Some studies have been made of the kinetics of transformation of the precursor to the sulfide. Montano et al. [5,6] used *in situ* Mössbauer spectroscopy to study the decomposition of pyrite, to pyrrhotite and H_2S, in hydrogen and under liquefaction conditions. It was found that the onset of the transformation to pyrrhotite occurs at ~300°C and is nearly complete at ~400°C. The activation energy of the transformation decreased with decreasing particle size. Larger pyrite particles were reported to break during the transformation yielding smaller pyrrhotite particles. It was concluded that both H_2S and pyrrhotite are active as catalysts for the liquefaction process. Others have attributed the catalytic activity of pyrite to H_2S alone[11], arguing that the low surface area of pyrite should make it a very poor catalyst. This view agrees with the finding that pyrite and pyrrhotite do not exhibit any catalytic effect for the gasification of graphite[14]. The view of a synergistic effect between pyrrhotite and H_2S has been reached by other workers using both pyrite and iron oxide[10].

In a study of the liquefaction of a Victorian brown coal [8l], using hematite, iron carbonyl, and impregnated iron acetate as catalyst precursors, it was concluded that, in the absence of added sulfur, the active form of the iron catalyst was reduced α-Fe. This concurs with the results of a study which found that metallic iron promoted the catalytic hydrogenation of graphite at temperatures below 1000 °C while pyrite and pyrrhotite showed no catalytic activity[14]. More recently, Weng et al.[15] have proposed that, while a synergistic effect between pyrrhotite and H_2S promotes coal liquefaction, γ-Fe is a more active catalyst than pyrrhotite. The fact that a substantial amount of Fe_3C was also formed during the reaction may indicate that insufficient sulfur was present for conversion of the precursor to pyrrhotite. This may be the reason for the γ-Fe formation.

As this brief summary indicates, the relationship between the phase of the iron catalyst and its activity is not fully understood. Neither is there any clear information

about the kinetics of precursor sulfiding, and the factors which influence this reaction. The relevance of these statements is that, even assuming that iron sulfide is an active liquefaction catalyst, the active phase may not be present during some of the critical initial reactions of coal dissolution.

The purposes of this work are to attempt to resolve\ these questions through: examining the effect of nanoscale iron carbide catalyst on coal liquefaction: determining the kinetics of *in-situ* sulfiding of the iron carbide; and comparing the performance when the catalyst is added in the form of nanoscale pyrrhotite. Both phases of the iron will be formed by a laser pyrolysis technique, described in detail elsewhere[13], which will ensure that the precursor particles have approximately the same size distribution. Previous studies have shown that the Fe_7C_3 particles transform to pyrrhotite, in the presence of added sulfur under liquefaction conditions, while retaining their small size[13]. By comparing the activity of the presulfided catalyst to the catalyst sulfided *in situ* , the relative activity of the two may be defined. This will allow a better appreciation of the importance of sulfiding kinetics, and the attainment of the active phase, to be determined.

EXPERIMENTAL

The coal used is a -200 mesh subbituminous Black Thunder coal which is stored in sealed foil bags prior to use, in order to reduce the effects of air oxidation. The native iron content of the coal is 0.17wt%. In liquefaction experiments 3 grams of coal and 5 grams of tetralin are charged into a 50 ml stainless steel tubing bomb reactor. The catalyst loading is 1 wt% Fe to coal. The reactors are constructed with a horizontal orientation to reduce any mass transfer limiting effects. Dimethyl disulfide (DMDS) is added at 120% of the calculated amount required for transformation of the precursor to pyrite. The sealed bombs are purged and pressurized with hydrogen to 1000 psig (cold) prior to reaction.

The bombs are agitated vertically at ~400 cycles/min while immersed in a heated fluidized sand bath. The reactions are carried out for up to 30 minutes, and at temperatures between 385°C and 415°C. Following reaction, the tubing bomb is removed from the heated sand bath and quenched in a cool sand bath. A gas sample is taken from the cooled reactor and analyzed by GC.

The products of the liquefaction experiments are analyzed by solubility class. The reactor contents are extracted with THF to determine the total conversion to THF soluble products. The THF solubles are then precipitated with pentane. The pentane soluble product is defined as the oil fraction while the insoluble portion is defined as the preasphaltene + asphaltene fraction. The THF insoluble fraction is defined as the IOM fraction. The gas yield is determined by GC and the oil yield is determined by difference.

The spent catalyst is contained in the IOM fraction and is characterized by XRD and Mössbauer spectroscopy to determine the phase and approximate size of the iron based catalyst after reaction.

RESULTS

In order to determine the behavior of the iron carbide particles under liquefaction conditions, tubing bomb experiments were carried out in the absence of added coal. As reported elsewhere[13], it was determined by XRD that the iron carbide particles transform to pyrrhotite in the presence of added sulfur within 30 min at 385°C. Further, analysis of TEM micrographs show that the particles retain their small size and relatively narrow size distribution, with the exception of the formation a few larger crystallites.

In liquefaction studies using a subbituminous Wyodak coal the iron carbide showed moderate catalytic activity, similar to that of iron pentacarbonyl. The catalyst loading in both cases was 1 wt% Fe. The iron carbide increased the total conversion by ~10% over the thermal baseline in the temperature range from 350°C to 440°C. Further, the catalyst caused an apparent increase in the selectivity to oils over the temperature range ~350°-400°C.

The method of production of the nanoscale iron carbide particles by laser pyrolysis has been reported elsewhere.[13] A modification of this process was used to produce the nanoscale pyrrhotite. A reactant gas stream of ethylene and hydrogen sulfide is intersected with the beam from a tunable CO_2 laser. The pyrrhotite particles are formed in the small pyrolysis zone formed at this intersection. The size of the particles can be controlled by adjusting the reaction parameters. XRD has identified the phase of the particles as $Fe_{(1-x)}S$ with an average diameter of ~10nm. Work is currently in progress to determine the catalytic activity of the nanoscale pyrrhotite particles as well as their behavior during the liquefaction process.

SUMMARY

The results of this study will allow the kinetics of the transition of iron carbide to the sulfide to be determined, and whether the transformation is sufficiently rapid so that an active catalyst is present during coal dissolution. By using two different catalysts produced by the same technique the influence of size effects on the activity are reduced. XRD and Mössbauer spectroscopy are used to determine the phase of the catalyst after the reaction. The relative importance of attainment of the active phase during the initial stages of liquefaction will be discussed.

ACKNOWLEDGEMENTS

This work was supported in part by the Department of Energy through the Consortium for Fossil Fuel Liquefaction Science DE-FC22-90PC90029 (PCE, XXB).

REFERENCES

1) Wu W R W, Storch H H, Hydrogenation of Coal and Tar, Bulletin 633, Washington, DC, USA, US Dept of the Interior, Bureau of Mines, 195pp, 1968

2) Herrick D E, Tierney J W, Wender I, Huffman G P, Huggins F E, *Energy & Fuels* **4,** 231-6,1990

3) Suzuki T, Yamada O, Takahashi Y, Watanabe Y, *Fuel Proc. Tech.*, **10,** 33-43, 1985

4) Sweeny P G, Stenberg V I, Hei R D, Montano P A, *Fuel*, **66**, 532-41, 1987

5) Montano P A, Vaishnava P P, King J A, Eisentrout E N, *Fuel*, **60**, 712-6, 1981

6) Montano P A, Bommannavar A S, Shah V, *Fuel*, **60**, 703-11, 1981

7) Cook P S, Cashion J D, *Fuel*, **66**, 669-77, 1987

8) Cook P S, Cashion J D, *Fuel*, **66**, 661-8, 1987

9) Kamiya Y, Nobusawa T, Futamura S, *Fuel Proc. Tech.*, **18,** 1-10, 1988

10) Wang L, Cui Z, Liu S, *Fuel*, **71**, 755-9, 1992

11) Lambert J M Jr, *Fuel*, **61**, 777-8, 1982

13) Hager G T, Bi X X, Derbyshire F J, Eklund P C, Stencel J M, ACS Div. of Fuel Chem. Preprints, **36**(4) 1900-8, 1991

14) Cypres R, Ghodsi M, Stocq R, *Fuel*, **60**, 247-50, 1981

15) Weng S, Wang Z, Gao J, Cheng L, Wu Z, Lin D, Yu Y, Zhao C, *Hyperfine Interactions*, **58**, 2635-39, 1990

COAL-LIQUEFACTION CATALYSTS FROM FERRIC SULFIDE DISPROPORTIONATION

Dady B. Dadyburjor, W.R. Stewart, A.H. Stiller,
C.D. Stinespring, J.-P. Wann and J.W. Zondlo
Department of Chemical Engineering, P.O. Box 6101
West Virginia University
Morgantown, WV 26506-6101

Keywords: Catalysis, Coal liquefaction, Ferric sulfide disproportionation

INTRODUCTION

The use of iron-based catalysts of small particle sizes in the liquefaction of coal is widespread in laboratories and in practice due to the cost-efficiency of the catalyst and the ability of the small particles to penetrate the pore structure of the coal, at least to some extent. Of the iron-based catalysts, pyrite (PY, FeS_2) is found indigenously in coal and has a well-documented ability [1] to enhance liquefaction rates. PY is known [2] to be converted to nonstoichiometric pyrrhotite (PH, FeS_x, $x \approx 1$) under hydrogen atmospheres at high temperatures and pressures, conditions expected in liquefaction. Whether PY or PH or a combination of the two is the catalytically active agent is a matter of current debate.

We have developed mixtures of PY and PH of small crystallite size. The mixtures contain different PH stoichiometries, and different amounts of PH and PY in intimate contact. The expectation is that the different valencies of Fe in atomic-range proximity give rise to a very efficient catalyst. These mixtures are made by disproportionating ferric sulfide (Fe_2S_3) at various temperatures and for various times. The PH/PY ratio and the value of x defined above change with these disproportionation parameters.

EXPERIMENTAL PROCEDURE

Ferric sulfide is prepared by mixing stoichiometric amounts of ferric chloride and sodium sulfide in a cold room below 5°C. The formation of ferric sulfide is instantaneous, following the reaction:

$$2FeCl_3 \cdot 6H_2O + 3Na_2S \cdot 9H_2O \longrightarrow Fe_2S_3 + 6NaCl + 39H_2O$$

PH, PY and elemental S are the products of disproportionation, through a general reaction of the type:

$$Fe_2S_3 \longrightarrow \alpha\ FeS_x + \beta\ FeS_2 + \gamma S$$

The solid is washed to remove NaCl and dried. A portion of the resulting solid is separated into PH (soluble in 6M HCl) and PY (soluble in 8M HNO_3), and the amount of Fe in each of these sulfide forms is analyzed by atomic absorption (AA). The rest of the solid is mixed with coal, solvent tetralin and CS_2 presulfider for the liquefaction runs. Occasionally the solid is analyzed by X-ray diffraction (XRD) and Auger Electron Spectroscopy (AES).

Liquefaction runs were carried out in a batch tubing-bomb reactor with vertical agitation. Most experiments were performed on DECS-17 coal, a low-PY, high-exinite material. After liquefaction, the solid is analyzed for

conversion (THF-soluble material) and asphaltenes/preasphaltenes (THF-soluble, hexane-insoluble material). The amount of oil (+ gas) is obtained by difference. The THF-insoluble solid is analyzed for PH and PY.

RESULTS

Ratios of pyrrhotite to pyrite (PH/PY) in the products of Fe_2S_3 disproportionation are shown as a function of disproportionation temperature, T_d, in Table I. Note that elemental S is not shown. Table I indicates that the room-temperature disproportionation yields only PH, for all practical purposes. Increasing T_d increases the relative amount of PY in the solid. Only a few S peaks are visible in the X-ray diffraction XRD pattern for the room-temperature case; presumably the PH crystallites are too small to exhibit peaks. Disproportionation at a temperature T_d = 100°C shows significant PY peaks but smaller S peaks; again the PH crystallites are X-ray-invisible. When T_d = 200°C, the PH crystallites are large enough to exhibit peaks, PY peaks are larger than at T_d = 100°C, and S peaks are vanishingly small.

Auger electron spectra for the PH/PY mixture after T_d = 200°C are shown in Figure 1. The shape of the Fe line at around 40 eV indicates that PH of composition Fe_7S_8 (x = 1.143) is present. Further, the line shape for S indicates that the elemental form is present. The intensity ratios of the S (LVV) peak to the Fe (LMM) are plotted in Figure 2 as a function of the ratio S/Fe for standard samples of FeS_2 and Fe_7S_8. Also shown in Figure 2 is the intensity ratio for the product corresponding to T_d = 200°C. This allows one to estimate the amount of surface S (elemental and ionic) to surface Fe for the disproportionated product.

The PH/PY ratio of the catalyst changes after liquefaction. As can be seen in Table I, the changes depend upon both T_d and T_ℓ. Table II shows the changes in the S/Fe ratio in the iron-based catalyst after liquefaction at T_ℓ = 350°C as a function of T_d.

In Figure 3 are plotted the overall conversion, asphaltene/preasphaltene yield and oil (+ gas) yield for DECS-17 coal as a function of the S/Fe ratio of the iron-based catalyst after liquefaction at T_ℓ = 350°C. Other choices of the independent variable obviously exist, yet this one appears to give linear relationships for conversion and yields. Results for the unsulfided catalysts, and for liquefaction at T_ℓ = 400°C with sulfided and unsulfided catalysts, have been tabulated elsewhere [3]. We did not test catalyst prepared at disproportionation temperatures higher than 200°C for conversion of DECS-17 coal. However, previous work [4] using Humphrey mine coal (Pittsburgh No. 8 seam) indicates that catalysts corresponding to a PH/PY ratio of unity (T_d = 200°C) have higher conversions and oil (+ gas) yields than those corresponding to larger and smaller ratios (T_d = 100°C, 250°C). These results are shown in Figure 4. Because of the superior performance of the catalyst formed by disproportionation at 200°C for 1 h, we concentrated on this catalyst for further evaluation.

To investigate the efficacy of catalyst-coal mixing, a catalyst impregnation procedure was attempted and conversions and yields were compared to those from the "standard" catalyst preparation procedure described above. In the impregnation procedure, an aqueous solution of $FeCl_3$ was sonicated with coal, then Na_2S was added, followed by additional sonication. After

disproportionation at 200°C for 1 h, the solid was washed with distilled water to remove NaCl, dried and then placed in the liquefaction reactor with tetralin and CS_2. The conversion and oil (+ gas) yield after liquefaction at T_ℓ = 350°C for 1 h are shown in Figure 5 as catalyst preparation IDW. Also shown in Figure 5 are liquefaction results for preparation procedure IWD, wherein the washing step was carried out between impregnation and disproportionation. Comparing the results of these procedures with the "standard" procedure, labelled DWM, shows that impregnation of the catalyst yields no particular advantage.

Also shown in Figure 5 are the effects of various NaCl-washing techniques on liquefaction. In procedure DNM, the catalyst was mixed directly after disproportionation, without any washing step. Conversions and yield are noticeably lower than DWM, where the washing step is not omitted. Finally, in procedure DWAM, the catalyst was disproportionated and washed (as in DWM), but then a calculated amount of NaCl was added to the solid before mixing with coal. The liquefaction results here are very similar to those where washing was eliminated, thus indicating that the washing step eliminates only the NaCl. In Figure 5, NC represents the results for thermal liquefaction, with no catalyst addition.

Figure 6 shows the effect of catalyst loading on the overall conversion and the yield of oil (+ gas). The loading of the PH/PY mixture catalyst affects the conversion and oil (+ gas) yield of DECS-17 coal in a nonlinear manner. The conversion increases for upto 1 percent loading; at higher loadings, the conversion continues to increase but to a lesser extent. At low catalyst loadings, the yield of oil (+ gas) is less than under non-catalytic conditions. The yield is a minimum around 1 percent loading, after which the yield increases.

Finally, it is worth comparing the disproportionated catalyst with other iron-based catalysts. Figure 7 shows the overall conversion and the oil (+ gas) yield for the case of no catalyst (NC), the catalyst mixture after T_d = 200°C (DFS), and an iron oxide catalyst, FeOOH, developed by Mobay Corporation and provided by Dr. Farcasiu, USDOE/PETC. Results of this catalyst are labelled IO in Figure 7. Liquefaction in each case was at T_ℓ = 350°C for 1 h. For DFS and IO, catalyst was added corresponding to 0.5 percent Fe. The DFS catalyst was prepared according to the "standard" procedure described above. Figure 7 shows that conversions for the two sulfided catalysts are comparable and greater than the (sulfided) NC case. Unsulfided IO is comparable to the unsulfided NC. Sulfiding improves IO considerably. The yields of oil (+ gas) with both catalysts are smaller than for the NC case, with the DFS yield being somewhat less than the IO yield. This is consistent with Figure 6 which shows the oil (+ gas) yield decreasing for small additions of catalyst (less than 1 percent).

CONCLUSIONS

Hydrothermal disproportionation of ferric sulfide yields a mixture of iron sulfides and elemental sulfur. The sulfides, FeS_2 and various pyrrhotites FeS_x, are present as intimately mixed crystallites in small particles. The relative amount and composition of the FeS_x can be controlled by varying the time and temperature of disproportionation. Thus these iron sulfides are suitable catalysts for coal liquefaction. The activity and selectivity of

these catalysts are comparable to those of other iron-based catalysts.

ACKNOWLEDGMENTS

The work was conducted under U.S. Department of Energy Contract No. DE-FC22-90PC90029 under the Cooperative Agreement to the Consortium for Fossil Fuel Liquefaction Science. The authors gratefully acknowledge the support.

REFERENCES

1. Shah, Y.T., Reaction Engineering in Direct Coal Liquefaction, Addison-Wesley, Reading, MA (1981).

2. Jagadeesh, M.S. and M.S. Seehra, J. Phys. D 14, 2153 (1981); Montano, P.A., A.S. Bommannavar and V. Shah, Fuel 60, 703 (1981).

3. Stansberry, P.G., J.-P. Wann, W.R. Stewart, J. Yang, J.W. Zondlo, A.H. Stiller and D.B. Dadyburjor, Fuel, accepted (1992).

4. Stansberry, P.G., J. Yang and J.-P. Wann, Paper presented at AIChE Annual Meeting, Los Angeles, CA (1991).

TABLE I

Pyrrhotite/Pyrite (PH/PY) Ratio Before and After Liquefaction as Functions of Disproportionation Temperature (T_d) and Liquefaction Temperature (T_ℓ).

T_d [°C]	PH/PY Ratios		
	Before Liquefaction	After Liquefaction	
		T_ℓ = 350°C	T_ℓ = 400°C
25	286	2.5	8.4
100	1.8	5.7	3.2
200	0.87	0.38	0.13

TABLE II

Final S/Fe Ratio in PH/PY Mixtures After Liquefaction at T_ℓ = 350°C

T_d [°C]	S/Fe
25	1.3
100	1.4
200	1.7

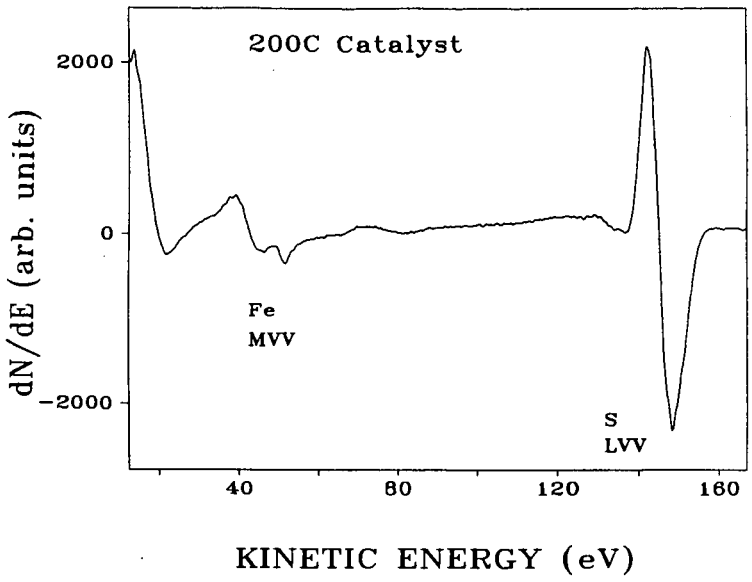

Figure 1. Auger electron spectrum for disproportionated catalyst, T_d = 200°C.

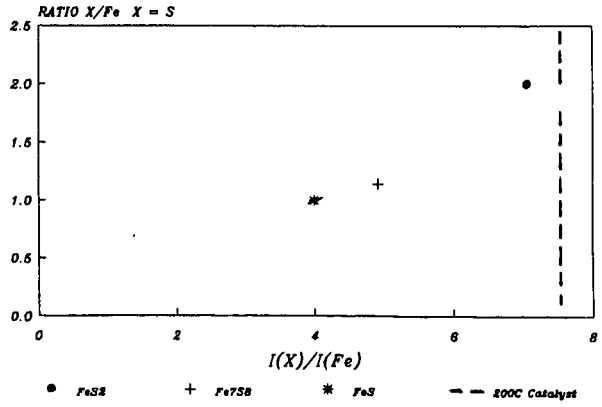

Figure 2. Sensitivity factors of Fe and S for FeS_2, Fe_7S_8, and disproportionated catalyst, T_d=200°C.

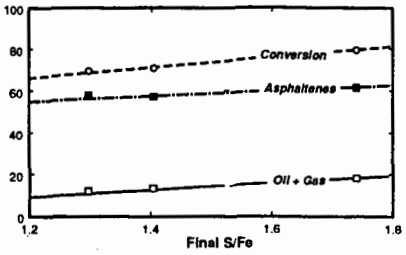

Figure 3. Conversion and yields of preasphaltenes/asphaltenes and oil(+gas) from DECS-17 coal as functions of the final S/Fe ratio of catalyst.

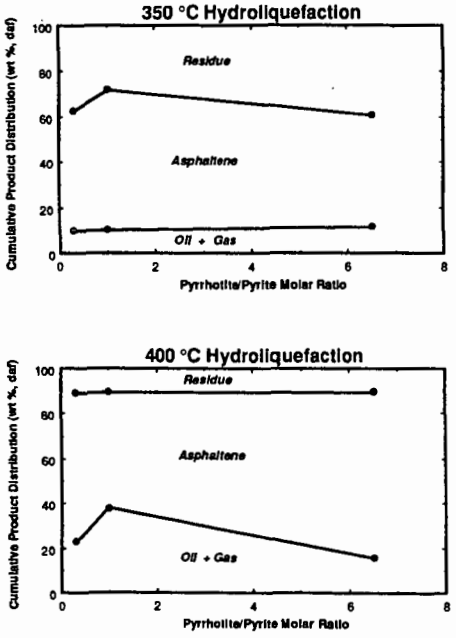

Figure 4. Conversion and yield of oil (+gas) as functions of PH/PY for liquefaction of Humphrey Mine coal [4].

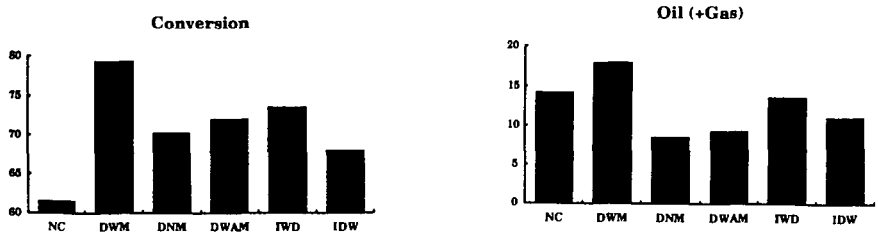

Figure 5. Conversion and yield of oil(+gas) for various procedures of catalyst manufacture. See text for nomenclature.

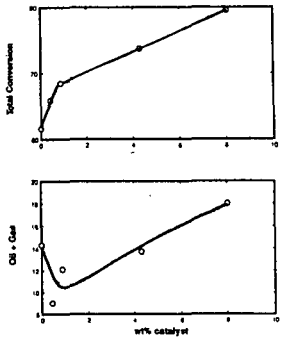

Figure 6. Conversion and yield of oil(+gas) as functions of catalyst loading.

Figure 7. Comparison of conversion (left) and yield of oil(+gas) (right) over disproportionated catalyst (DFS) and over iron oxide catalyst (IO).